Poultry Science®

Gut microbiota and serum metabolome reveal the mechanism by which TCM polysaccharides alleviate salpingitis in laying hens challenged by bacteria

Jiali Liu,* Pupu Yan,* Yana Li,* Jie Yu,* Yongxi Huang,* Ruonan Bai,* Man Liu,* Ning Wang,* Lian Liu,* Jun Zhu,* Junhao Xiao,* Liwei Guo,*,[1] Guoping Liu,* Fuxian Zhang,* Xiaolin Yang,* Bin He,† Jianguo Zeng,‡ and Xiaoqin Zeng§

*College of Animal Science and Technology, Yangtze University, Jingzhou, Hubei, China; †Institute of Animal Husbandry and Veterinary Medicine, Wuhan Academy of Agricultural Sciences, Wuhan, Hubei, China; ‡College of Veterinary Medicine, Hunan Agricultural University, Changsha, Hunan, China; and §The First Affiliated Hospital of Yangtze University, Jingzhou, Hubei, China

ABSTRACT This paper aimed to evaluate the effect of 3 kinds of TCM polysaccharides instead of antibiotics in preventing salpingitis in laying hens. After feeding the laying hens with Lotus leaf polysaccharide, *Poria* polysaccharide, and *Epimedium* polysaccharide, mixed bacteria (*E. coli* and *Staphylococcus aureus*) were used to infect the oviduct to establish an inflammation model. Changes in antioxidant, serum immunity, anti-inflammatory, gut microbiota, and serum metabolites were evaluated. The results showed that the 3 TCM polysaccharides could increase the expression of antioxidant markers SOD, GSH, and CAT, and reduce the accumulation of MDA in the liver; the contents of IgA and IgM in serum were increased. Decreased the mRNA expression of TLR4, NFκB, TNF-α, IFN-γ, IL1β, IL6, and IL8, and increased the mRNA expression of anti-inflammatory factor IL5 in oviduct tissue. 16sRNA high-throughput sequencing revealed that the 3 TCM polysaccharides improved the intestinal flora disturbance caused by bacterial infection, increased the abundance of beneficial bacteria such as *Bacteroides* and *Actinobacillus*, and decreased the abundance of harmful bacteria such as *Romboutsia, Turicibacter*, and *Streptococcus*. Metabolomics showed that the 3 TCM polysaccharides could increase the content of metabolites such as 3-hydroxybutyric acid and isobutyl-L-carnitine, and these results could alleviate the further development of salpingitis. In conclusion, the present study has found that using TCM polysaccharides instead of antibiotics was a feasible way to prevent bacterial salpingitis in laying hens, which might make preventing this disease no longer an issue for breeding laying hens.

Key words: TCM polysaccharides, salpingitis, immunity and antioxidants, gut microbiota, serum metabolome

2024 Poultry Science 103:103288
https://doi.org/10.1016/j.psj.2023.103288

INTRODUCTION

Salpingitis is one of the major problems faced by laying hens worldwide, characterized by rapid and easy large-scale outbreaks (Pors et al., 2014). Salpingitis can cause a decrease in egg production and quality and a large area of sudden death due to inflammation spreading to the abdominal cavity in laying hens (Johnson et al., 2011). At autopsy, tubal lesions can be observed, including blockage, necrosis, and ulceration, and in more severe cases, white-caseated inflammatory secretions can also be observed (Fang et al., 2021). In China, most laying hen farm faces the threat of salpingitis. These causes are various, including excessive egg production due to uneven feed supply, eggshell rupture in the oviduct damage (Bisgaard, 1995), stress reactions, and various diseases (including avian influenza, Newcastle disease, infectious bronchitis, avian leukemia, and egg drop syndrome), and so on (Shalaby et al., 1994; Bonfante et al., 2018; Zhang et al., 2020). In addition, the poor hygiene of the poultry house and the invasion of the cloacal of laying hens by gram-negative bacteria, including *Salmonella* and *Escherichia coli* to infect the oviduct are the leading inducement causes of the disease (Wang et al., 2020). Before 2018, the primary plan to control salpingitis was to add antibiotics to the feed in China (Wang et al., 2020), which alleviated the outbreak of the disease to a certain extent. However, there was an obvious problem—the residue of antibiotic drugs and the emergence of drug-resistant bacteria, which could be fatal to human life (Bacanlı and Başaran, 2019). Therefore, adding antibiotics to feed has been completely

Received October 19, 2023.
Accepted November 13, 2023.

[1]Corresponding author: guolw@yangtzeu.edu.cn

banned in China since 2018 (Walsh and Wu, 2016). However, the prevention and treatment of salpingitis in laying hens is still an urgent problem to be solved.

Traditional Chinese medicine (**TCM**) polysaccharides are a class of active polysaccharides extracted from Chinese herbal medicine with a wide range of sources (Zeng et al., 2019). As active substances, TCM polysaccharides can improve physiological functions, protect the immune organs, activate immune cells, release cytokines, and modulate the gut microbiome (Zeng et al., 2019; Sun et al., 2022). *Lotus leaf* is a medicinal and edible plant, and polysaccharide is one of its active ingredients (Wu et al., 2022). Lotus leaf polysaccharide has many effects, including weight loss, anti-inflammatory, antioxidation, antibacterial, and immune enhancement (Zheng et al., 2022). In the poultry breeding industry, lotus leaf and its active components can increase the content of serum immunoglobulin and the expression level of anti-inflammatory factors, thereby improving poultry's immunity and disease resistance (Cheng et al., 2021). *Poria cocos* has been used as a folk medicine and functional food in China for over 2000 years (Zhang et al., 2022). *Poria cocos* have the effects of reducing water and dampness, strengthening the spleen, and calming the heart. It has antispleen enlargement, enhanced phagocytosis of macrophages, and other effects (Tian et al., 2019), and polysaccharide is the main component of the sclerotia of *Poria cocos*. *Epimedium* polysaccharides (**EP**) have apparent effects on antivirus, antioxidation, antitumor, antiaging, and immune regulation (Wang et al., 2017). In addition, EP also had an anti-immunosuppressive effect (Guo et al., 2012). Despite the advantages of TCM polysaccharides, there are few reports on the prevention and treatment of salpingitis in laying hens by TCM polysaccharides.

This study aimed to verify the preventive effects of 3 TCM polysaccharides on salpingitis. The salpingitis laying hens' specific immune, antioxidant, and inflammatory factors were evaluated, focusing on the study of gut microbiota and serum metabolome to explore the potential relationship between TCM polysaccharides and intestinal microbiome and metabolites.

MATERIALS AND METHODS

Ethics Statement

Animal experiments in this study were performed according to the Regulations on Administration of Animal Experiments (Ministry of Science and Technology of China, Approval No. 2006-398) and approved by the Animal Ethics Committee of Yangtze University (Jingzhou, Hubei, China).

Sources of Polysaccharides and Amoxicillin

Lotus leaf polysaccharides (**LLP**), *Poria cocos* polysaccharides (**PCP**), and EP were extracted according to previously described methods (Cheng et al., 2013; Zhao et al., 2023) and stored in the Laboratory of Chinese Veterinary Medicine, Yangtze University. The phenol sulfuric acid method determined the polysaccharide concentration and adjusted to 20 mg/mL with pure water (Rasouli et al., 2014). Amoxicillin (Nanhua Qianmu Biotechnology Co., Ltd., Henan, China).

Animals, Diets, and Management

Hubei Fuqiang Poultry Breeding Company provided vaccinated, disease-free, 300-day-old Hy-line brown laying hens. One hundred and twenty healthy laying hens were randomly placed in 500×350×700 mm cages. The temperature was 26°C ± 2°C, moderate 55 ± 5%, light for 16 h, and drinking water and diet were changed every 8 h. After 7 d of adaptive feeding, they were divided into 6 groups: blank group: basic diet (without polysaccharide and drugs); Model group: basic diet (after 14 d, *Staphylococcus aureus* and *Escherichia coli* were administered via cloaca); LLP group: basic diet supplemented with Lotus leaf polysaccharide 20 mg/kg (after 14 d, *Staphylococcus aureus* and *Escherichia coli* were administered via cloaca); PCP group: basic diet supplemented with *Poria cocos* polysaccharides 20 mg/kg (after 14 d, *Staphylococcus aureus* and *Escherichia coli* were administered via cloaca); EP group: basic diet supplemented with EP 20 mg/kg (after 14 d, *Staphylococcus aureus* and *Escherichia coli* were administered via cloaca); AMX group: basal diet supplemented with Amoxicillin 2.5 g/kg (after 14 d, *Staphylococcus aureus* and *Escherichia coli* were administered via cloaca). Basic feed composition levels were located in Table 1.

On day 21 of the experiment, the hens were euthanized by spinal dissection after deep anesthesia. Blood, liver, oviduct, and ileum contents were collected to evaluate serum immune and liver antioxidant levels, oviduct pathological changes, inflammatory factor mRNA, ileal microbial composition, and serum metabolome.

Laying Performance

During the polysaccharide feeding and bacterial infecting cycles, record the number of eggs laid daily, including damaged eggs. Compare the effects of polysaccharides and bacteria on laying performance.

Table 1. Basal diet composition and nutrition table.

Ingredient	Content (%)	Nutrient levels	Content (%)
Corn	55.7	Crude protein	15.5
Secondary powder	8.0	Lysine	0.65
Soybean meal	11.5	Methionine	0.32
Peanut cake	8.0	Threonine	0.45
Fish meal	4.0	Crude fiber	7.0
Calcium hydrogen phosphate	1.2	Coarse ash	15.0
Stone powder	7.7	Calcium	3.5
Vegetable oil	3.0	Total phosphorus	0.35
Cypress of cotton	0.10	Water content	14.0
Additive	0.50		
salt	0.30		
Total	100		

The above analytical error was performed under the allowable error as determined by the feed test results of GB/t18823.

Pathological Changes of the Oviduct

Fresh tubal tissue from sample collection was fixed in 4% paraformaldehyde, dehydrated in ethanol gradients (75, 80, 90, 95, and 100%), transparent in xylene, and embedded in paraffin for serial sectioning. Stain tissue sections with hematoxylin and eosin (**H&E**). The pathological changes of the oviduct tissue were observed under the XD30A-RFL microscope (Sunny Optical Technology Co., Ltd., Zhejiang, China).

Serum-Specific Immunity

Let the collected blood stand at 37°C for 15 min and 4°C for 2 h to wait for serum precipitation. The sandwich ELISA kit (Lunchangshuo Biotechnology Co., Ltd., Xiamen, China) was used to detect the levels of IgA and IgM in the serum.

Liver Oxidative Stress Levels

The levels of superoxide dismutase (**SOD**), malondialdehyde (**MDA**), glutathione (**GSH**), and catalase (**CAT**) were determined using the kit provided by Nanjing Jiancheng Bioengineering Research Institute. All tests were carried out in strict accordance with the instructions provided by the manufacturer. In general, GSH and MDA can react with specific substances at 37°C to produce yellow and red-brown colored substances. The content can be calculated after measuring the absorbance at a specific wavelength using a multimode microplate reader (Multiskan SkyHigh, Thermo Fisher Scientific, Massachusetts). SOD and CAT can reduce the content of chromogenic substances through specific reactions, and the content in the liver can be calculated by specific formulations.

Real-Time Quantitative PCR Analysis

The total RNA of the oviduct tissue was extracted using the TRIZOL kit (Biosharp, Hefei, China) and reversely transcribed into cDNA using the cDNA reverse transcription kit (Abconal, Wuhan, China). Real-time quantitative PCR (**RT-qPCR**) was used with the following program: 95°C for 3 min, 30 cycles of 95°C for 5 s, and 60°C for 30 s, with GADPH as an internal reference. The $2^{-\Delta\Delta CT}$ method was used to calculate the relative changes in mRNA. Primers were designed by Premier 5 software, with product scores greater than 98. The primer sequences were located in Table 2.

Microbial 16S rRNA Gene Sequencing

The CTAB/SDS method was used to extract total genomic DNA from the ileal contents. DNA concentration and purity were monitored using 1% agarose gels and diluting DNA to 1 ng/μL with sterile water. 16S rRNA was amplified using specific primers (F: CCTAYGGGRBGCASCAG; R: GGACTACNNGGGTATCTAAT). All PCR mixtures contained 15 μL of Phusion High-Fidelity PCR Master Mix (New England Biolabs), 0.2 μM of each primer, and 10 ng target DNA. Cycling conditions were consisted of a first denaturation step at 98°C for 1 min, followed by 30 cycles at 98°C (10 s), 50°C (30 s), and 72°C (30 s) and a final 5 min extension at 72°C.

Mix an equal volume of 1× loading buffer (containing SYBR Green) with PCR products and perform electrophoresis on 2% agarose gel for DNA detection. The PCR products were mixed in equal proportions, and then the Qiagen Gel Extraction Kit (Qiagen, Germany) was used to purify the mixed PCR products. Following the manufacturer's recommendations, sequencing libraries were generated with NEBNext Ultra IIDNA Library Prep Kit (Cat No. E7645). The library quality was evaluated on the Qubit@ 2.0 Fluorometer (Thermo Scientific) and Agilent Bioanalyzer 2100 system. Finally, the library was sequenced on an Illumina NovaSeq platform, generating 250 bp paired-end reads. Subsequently, after merging with dual-end read segments and quality control, effective Tags were obtained, denoise was performed with DADA2 or blur module in the QIIME2 software (Version QIIME2-202006) to obtain initial ASVs (Amplicon Sequence Variants), and then ASVs with abundance less than 5 were filtered out. Species annotation was performed using QIIME2 software to calculate the community composition of subordinate samples at different taxonomy levels: phylum, class, order, family, genus, and species. In order to study the phylogenetic relationship of each ASV and the differences of the dominant species among different samples, multiple sequence alignment was performed using QIIME2 software. Finally, the absolute abundance of ASVs was normalized using a standard sequence number corresponding to the sample with the least sequences. Subsequent analysis of alpha diversity and beta diversity were all performed based on the output normalized data.

Table 2. Primers for real-time quantitative PCR.

Gene	Primer sequence (5′−3′)
TLR4	F: TCCCAACCCAACCACAG
	R: GGATAACAAAGGCATCATAG
NFκB	F: ATGTCTCCATTTGGCATCTATTCA
	R: TCCTCACTTTCGGGCAGTATCT
TNF-α	F: CCGCCCAGTTCAGATGAGTT
	R: CAACCAGCTATGCACCCCA
IFN-γ	F: CTGACAAGTCAAAGCCGCAC
	R: TCAAGTCGTTCATCGGGAGC
IL1β	F:GCCTGCAGAAGAAGCCTCG
	R: GCCTGCAGAAGAAGCCTCG
IL6	F: AAATCCCTCCTCGCCAATCT
	R: AAATCCCTCCTCGCCAATCT
IL8	F:GCTGCTCTGTCGCAAGGT
	R: GAATGGATTTAGGGTGGA
IL5	F:GGACATGCTGGTAAGTTCCAT
	R: GGGATGGCCTCAGTTTGTCA

Serum Metabolome

Metabolite Extraction From Serum The serum stored at −80°C was thawed at 4°C, and 100 μL of the serum was transferred to a sterile, enzyme-free EP tube with

400 μL of the extract (methanol:acetonitrile = 1:1 (V/V) containing the isotope-labeled internal standard was mixed). The hybrid solution was vortexed for 30 s, sonicated for 10 min in 4°C water bath, and incubated for 1 h at −40°C to precipitate proteins. Then, the samples were centrifuged at 12,000 rpm (RCF =13,800 (g), R = 8.6 cm) for 15 min at 4°C. The supernatant was transferred to a fresh glass vial for analysis.

Test on Machine LC-MS/MS analyses were performed using a UHPLC system (Vanquish, Thermo Fisher Scientific) with a Waters ACQUITY UPLC BEH Amide (2.1 mm × 50 mm, 1.7 μm) coupled to Orbitrap Exploris 120 mass spectrometer (Orbitrap MS, Thermo). The mobile phase consisted of 25 mmol/L ammonium acetate and 25 mmol/L ammonia hydroxide in water (pH = 9.75) (A) and acetonitrile (B). The auto-sampler temperature was 4°C, and the injection volume was 2 μL. The Orbitrap Exploris 120 mass spectrometer was used for its ability to acquire MS/MS spectra on information-dependent acquisition (**IDA**) mode in the control of the acquisition software (Xcalibur, Thermo). The acquisition software continuously evaluated the full scan MS spectrum in this mode. The ESI source conditions were set as follows: sheath gas flow rate as 50 Arb, Aux gas flow rate as 15 Arb, capillary temperature 320°C, full MS resolution as 60,000, MS/MS resolution as 15,000, collision energy: SNCE 20/30/40, spray voltage as 3.8 kV (positive) or −3.4 kV (negative), respectively.

Data Processing The raw data were converted to the mzXML format using ProteoWizard and processed with an in-house program developed using R language and based on XCMS for peak detection, extraction, alignment, and integration. Then, an in-house MS2 database (BiotreeDB) was applied to metabolite annotation. The cutoff for annotation was set at 0.3. Subsequently, the preprocessed data were normalized, and cluster analysis, principal component analysis, and OPLS-DA analysis were performed. The differential metabolites were screened by unit and multivariate statistical analysis and further analyzed by bioinformatics.

Correlation Analysis Between Gut Microbiota and Serum Metabolome To visually reflect the differences in expression patterns of differential bacterial flora (based on *Lactobacillus Romboutsia, Bacillus, Turicibacter, Clostridium_sensu_stricto_1, Enterococcus, Pseudomonas, Helicobacter, Streptococcus, Staphylococcus, Chloroplast*, and *Rothia11*) and differential metabolites, correlation hierarchical clustering analysis was performed on the significantly different bacterial flora and metabolites, Euclidean distance matrix was calculated, and the differential metabolites and bacterial flora were clustered by complete linkage method. Bacterial groups and metabolites clustered within the same cluster have similar expression patterns and may be in relatively close reaction steps in the biological process.

Statistical Analysis

GraphPad Prism 9.0 (GraphPad Inc., LaJolla, CA) and SPSS 25.0 (SPSS Inc., Chicago, IL) were used to analyze the data. Compare the data between groups using 1-way variance (**ANOVA**) and explore the significance of the differences between groups using least significant difference (**LSD**). The analysis results were shown as mean ± standard deviation (**SD**), and when the P value was less than 0.05, the results were considered to have significant differences.

RESULTS

The Effect of Polysaccharide Feeding and Bacterial Infection on Egg Production Performance

As shown in Figure 1, during the normal feeding stage, there was no significant difference in egg

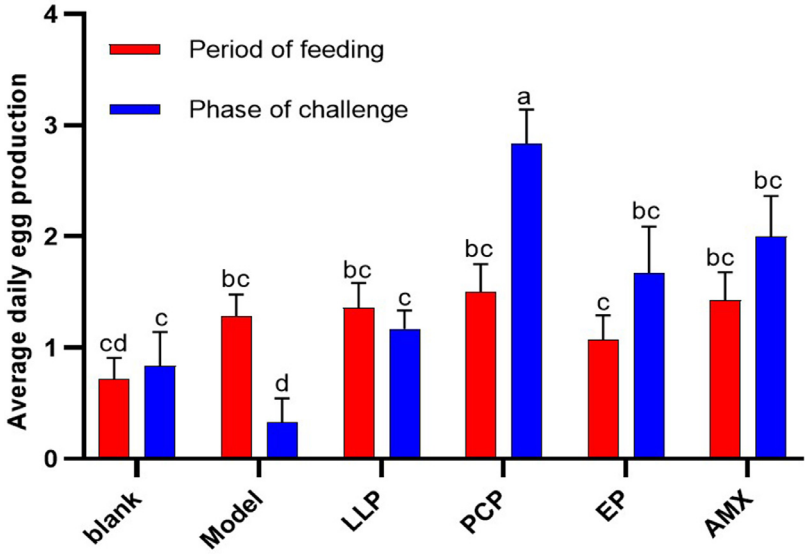

Figure 1. Average daily egg production of laying hens fed TCM polysaccharides and subjected to bacterial challenge (significant differences ($P < 0.05$) between groups with different superscripts a, b, c, and d).

production among all groups ($P > 0.05$). There was an upward trend in egg production rate in polysaccharide and AMX groups compared with the blank group. After the bacterial challenge, the number of eggs laid in the model group decreased sharply compared with the blank group ($P < 0.05$), while it did not show a decrease in the polysaccharides group. It was worth noting that compared with the model group, the number of eggs laid in the polysaccharide groups and the AMX group was still significantly higher even after bacterial challenge ($P < 0.05$), especially in the PCP group; it was higher than other groups ($P < 0.05$).

Appearance and Histopathology of the Oviduct

As shown in Figure 2, the oviduct tissue in the blank group, LLP group, and PCP group was complete, elastic, with abundant blood vessels, smooth yolk, and good shape, no pollution in the abdominal cavity, and no smell during on-site autopsy. Although the tubal tissue of the EP and AMX groups was intact, it was worth noting that there was fluid accumulation in the abdominal cavity of laying hens in both groups. In the model group, oviduct tissues showed typical pathological features, including blockage and necrosis, squeezed blood vessels, yolk rupture and accumulation, and odor during the field autopsy.

The pathological sections of the tubal tissue are shown in Figure 3. The tubal structure was complete in the blank group, with no inflammatory cell infiltration and tight tissue connections. The model group had more inflammatory cell infiltration, cell death, vacuolation and dispersion, and adhesion in the lumen. The tubal wall connection was complete in the LLP group, with some tissues scattered and unclear stratification. In the PCP group, the tissue structure was whole, the tubal epithelial cells were closely connected, and there was no inflammatory cell infiltration. In the EP group, the tubal wall structure was clear, and the tubal lumen was unobstructed. Scattered tissue was shown in the tubal lumen sporadically. In the AMX group, the tubal wall was intact, and the tissue was scattered, accompanied by a small amount of cell vacuolation.

Serum-Specific Immunity

The results of serum-specific immunity were shown in Figure 4A, B. Compared with the blank group, the contents of IgA and IgM in the model group were significantly downregulated ($P < 0.05$) after being subjected to bacterial attack. In contrast, those in the LLP and PCP groups were significantly increased compared with the model group ($P < 0.05$), especially the highest IgA and IgM contents in the LLP group. Although there was no significant difference between the EP and AMX groups compared with the model groups ($P > 0.05$), they also showed a recovery trend.

Effects of Different Polysaccharides on Antioxidant Levels in the Liver

Subsequently, antioxidant levels in the liver of laying hens attacked by bacteria after feeding with different polysaccharides were detected. The results of MDA were shown in Figure 4C. Compared with the blank group, MDA content in the model group increased sharply after bacterial invasion ($P < 0.01$). In LLP and PCP groups, it showed the best effect ($P < 0.05$). It was worth noting that although MDA content in the AMX group showed a downward trend, there was no significant difference ($P > 0.05$) compared with the model group.

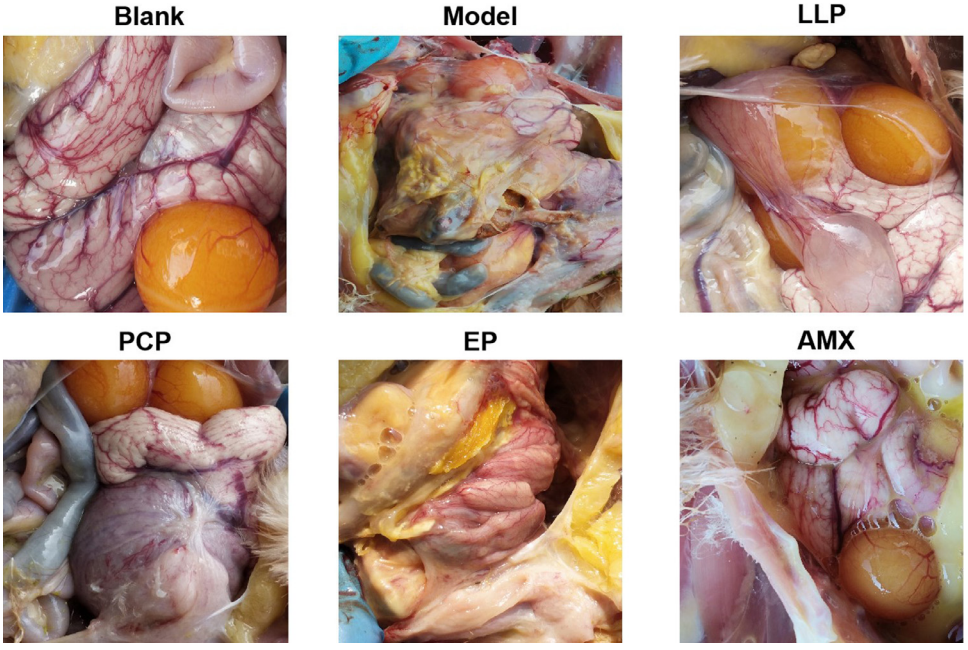

Figure 2. Laying hens fed TCM polysaccharides and subjected to bacterial challenge were examined visually by necropsy.

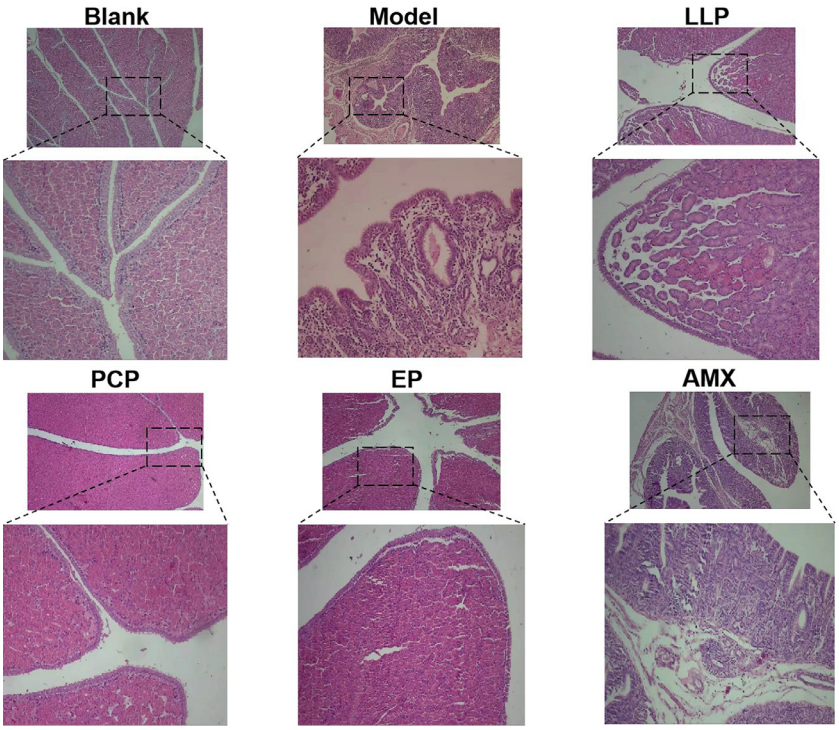

Figure 3. Pathological sections of laying hens fed TCM polysaccharides and subjected to bacterial challenge were examined.

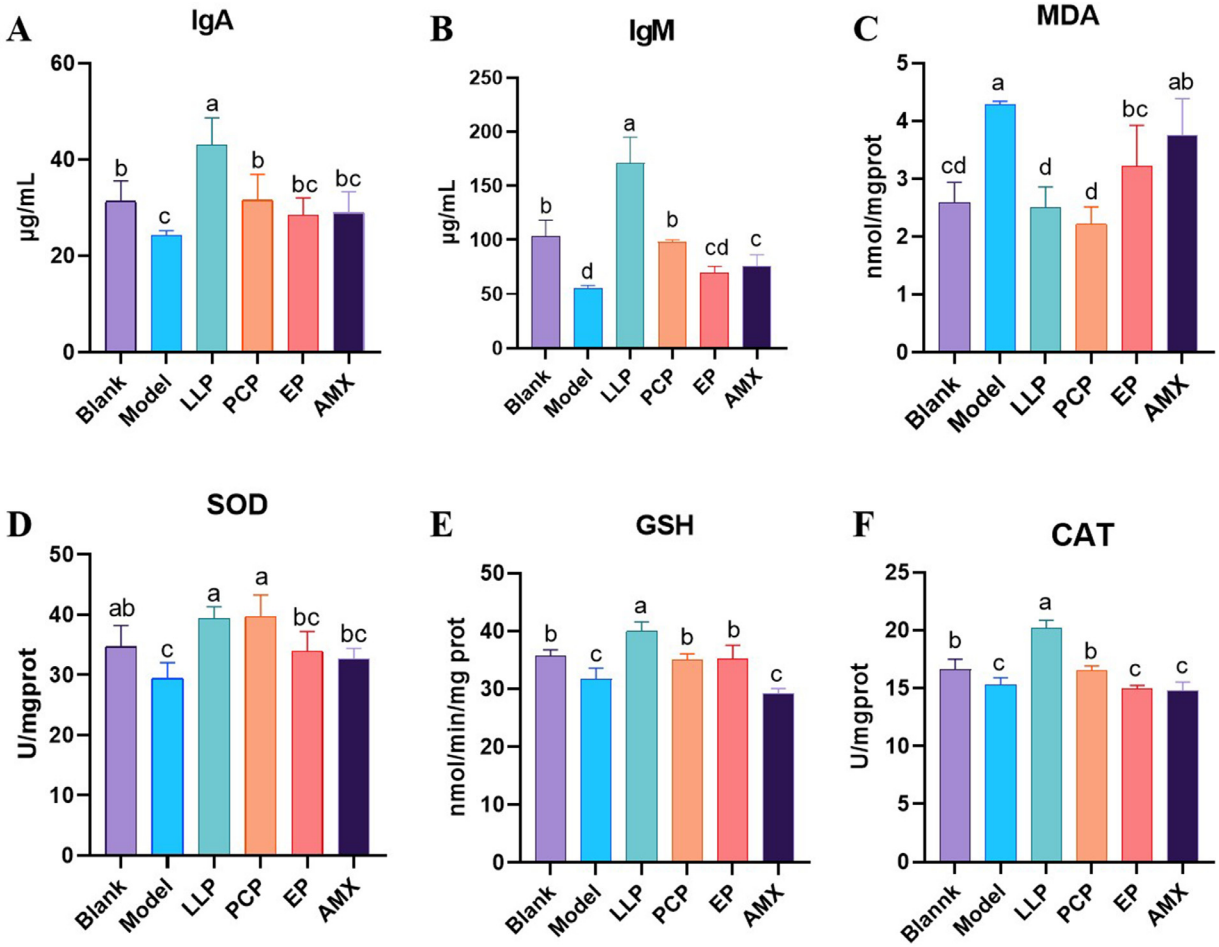

Figure 4. Serum-specific immunity and liver antioxidant levels. Serum IgA level (A), serum IgM level (B), liver MDA level (C), liver SOD level (D), liver GSH level (E) and liver CAT level (F) of hens fed polysaccharide and bacteria challenge. All experiments were repeated more than 3 times and presented as mean ± SD (significant differences ($P < 0.05$) between groups with different superscripts a, b, c, and d).

As shown in Figure 4D, the content of SOD in the model group was significantly decreased compared with that in the blank group ($P < 0.05$). Compared with the model group, the content of SOD in LLP and PCP groups showed a better upward trend. The EP and AMX groups did not reach a better level but had no significant difference compared with the blank group ($P > 0.05$).

GSH and CAT contents were shown in Figure 4E, F. Compared with the blank group, the content of GSH in the model group was significantly downregulated ($P < 0.05$), but compared with the model group, the contents of GSH in polysaccharide groups were significantly increased ($P < 0.05$). The content of CAT in the LLP and PCP groups was significantly different from that in the model group ($P < 0.05$). There was no significant difference between the EP and AMX groups ($P > 0.05$).

Effects of Different Polysaccharides on mRNA Levels Associated With Inflammation

To determine the effect of polysaccharides on salpingitis, the mRNA expression levels of related inflammatory signaling factors and cytokines were detected, as shown in Figure 5. After the mixed bacterial attack, compared with the blank group, the Model group expression levels of TLR4 (Figure 5A), NFκB (Figure 5B), TNF-α (Figure 5C), IFN-γ (Figure 5D), IL1β (Figure 5E), IL6, and IL8 (Figure 5G) were significantly increased ($P < 0.05$). Compared with the model group, the expression levels of these cytokines were significantly downregulated in EP and AMX groups ($P < 0.05$). The above inflammatory factors in LLP and PCP groups were the most significant downregulated ($P < 0.01$). In addition, Compared with the blank group, the expression of IL5 in the model group was significantly downregulated after bacterial infection ($P < 0.05$). Compared with the model group, the expression level of IL5 in the LLP and PCP groups was upregulated considerably ($P < 0.05$). The AMX group did not show an upward trend ($P > 0.5$), although the EP group showed the same result ($P > 0.5$), but there was an upward trend.

Composition of Intestinal Flora in Laying Hens Fed Polysaccharide

After data splicing and filtering, the statistical results were shown in Table 3. The results showed that the average sequence length of bacterial 16S rRNA was 418 bp, the Basic group of Q20 and Q30 was greater than 98 and 93%, and the average GC content was 51, sufficient to support the subsequent analysis.

The petal diagram of bacterial flora structure can represent the common and unique number of ASVs in each group under different polysaccharide and drug-feeding conditions and evaluate the differences and similarities degree between groups. The petal diagram as Figure 6A showed that there were 70 ASV in the 6 groups, 493 ASV in the blank group, 207 ASV in the model group, 487 ASV in the LLP group, 906 ASV in the PCP group, 367 ASV in the EP group and 384 ASV in AMX group. The number of ASVs in each polysaccharide group was higher than in the model group. The composition of phylum and genus of ileal microbial composition of laying hens is shown in Figure 6B. *Firmicutes, Proteobacteria, Bacteroidota*, and *Actinobacteriota* were the dominant microbiota in the ileum. As shown in Figure 6C to F, there was no significant difference in the abundance of *Firmicutes* in each polysaccharide group compared with the blank group ($P > 0.05$), and the abundance of *Proteobacteria, Bacteroidota*, and *Actinobacteriota* was

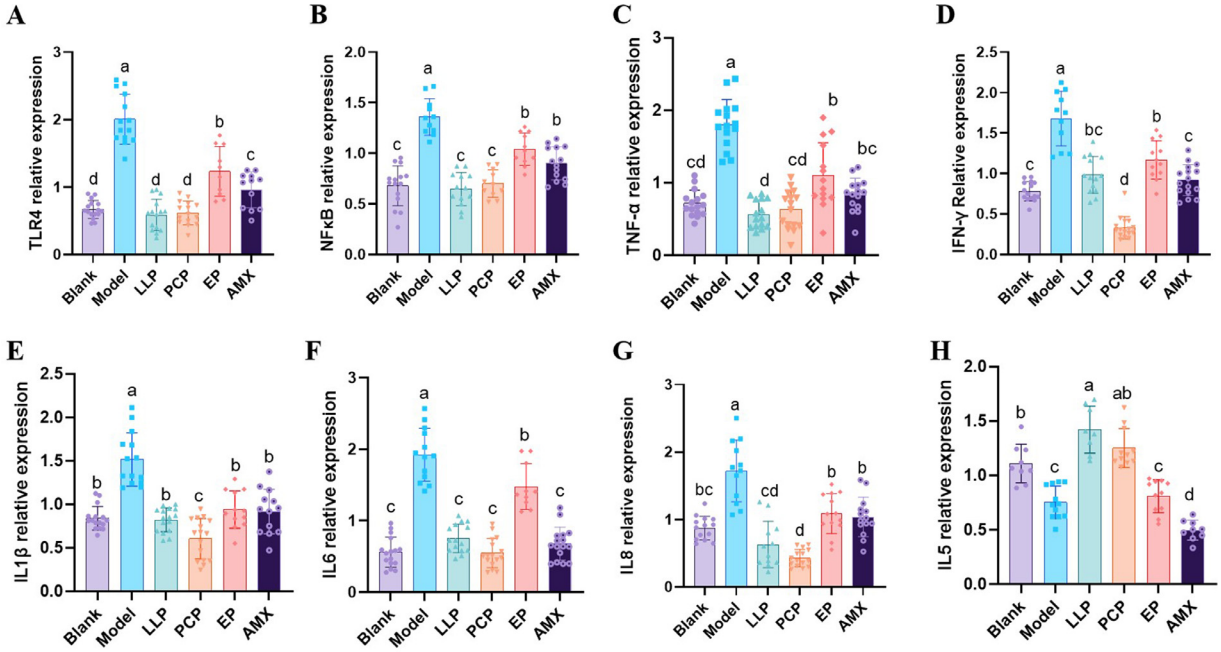

Figure 5. mRNA expression levels of related cytokines in oviduct tissues of laying hens. TLR4 (A), NFκB (B), TNF-α (C), IFN-γ (D), IL1β (E), IL6 (F), IL8 (G), and IL5 (H). All experiments were repeated more than 3 times and presented as mean ± SD (significant differences ($P < 0.05$) between groups with different superscripts a, b, c, and d).

Table 3. Data processing statistical results.

Group name	Qualified	Nochime	AvgLen	Q20	Q30	GC%	Effective%
Blank	76096	71639	421	97.91	93.34	51.36	88.96
Model	77179	72435	420	98.17	94.00	51.34	91.50
LLP	75029	69677	425	97.87	93.19	50.63	88.69
PCP	77432	69355	412	98.33	94.43	51.88	87.28
EP	79477	74748	423	97.68	92.72	50.14	91.21
AMX	77150	74212	405	98.26	94.10	52.93	90.69

Qualified is the sequence after Raw Tags filter low quality and short length; Nochime is the Tags sequence that is finally used for subsequent analysis after filtering chimeras, namely Effective Tags. The base is the number of bases in the final Effective Tags. AvgLen is the average length of Effective Tags; Q20 and Q30 are the percentages of bases in Effective Tags with base quality values greater than 20 (sequencing error rate less than 1%) and 30 (sequencing error rate less than 0.1%). GC (%) represents the content of GC bases in Effective Tags. Effective (%) represents the percentage of the number of Effective Tags to the number of Raw PE.

significantly downregulated in the model group ($P < 0.05$). Compared with the model group, the polysaccharide group had an upward trend in the abundance of the above bacteria, and the PCP group had the highest abundance ($P < 0.01$). It was worth noting that the AMX group did not show a good recovery trend ($P > 0.05$). The dominant bacteria at the genus level of ileum microorganisms were shown in Figure 6G, mainly including *Lactobacillus, Rombotusia, Bacillus, Turicibacter*, and *Acinetobacter*. Furthermore, the gut microbiota with significant differences were analyzed. Results were shown in Figure 6H to K. Compared with the blank group, there was no significant difference in *Lactobacillus* abundance in the model group ($P > 0.05$), but significantly increased in LLP and EP groups ($P < 0.05$), significantly decreased in AMX group ($P < 0.05$); the abundance of *Rombotusia* was significantly increased in the model and AMX groups ($P < 0.05$, $P < 0.01$), and was significantly decreased in the polysaccharide group ($P < 0.05$); the abundance of *Turicibacte* and *Streptococcus* was increased in the model and AMX groups ($P < 0.05$, $P < 0.01$), and significantly decreased in the polysaccharide group ($P < 0.05$).To further investigate the phylogenetic relationships of gene-level species, representative sequences of the top 100 genus were obtained by multiple sequence comparisons shown in Figure 6L. The gene-level genera of each group were mainly distributed in *Firmicutes* and *Lactobacillus* but less in the AMX group. In addition, the genus *Bamboo* was primarily distributed in the blank, LLP, and EP groups, while the genus *Longbrinus* was more distributed in the model and AMX groups. The representative sequence of the top 100 genera was obtained by multisequence comparison shown in Figure 6E to study the phylogenetic relationship of gene-level species further. The gene-level genus in each group except the AMX group was mainly distributed in phylum *Firmicutes* and genus *Lactobacillus*. In addition, the blank group, LLP, and EP groups were mainly distributed in the genus *Bacillus*. In contrast, in the model group and AMX group, there were more distributed in genus *Romboutsia*.

Analysis of α-Diversity and β-Diversity of Ileum Microorganisms

The obtained ASV feature sequences were analyzed by alpha diversity analysis, and Tukey and Kruskal-Wallis rank sum tests examined the species diversity differences between groups. The results of Chao1 (Figure 7A), Observed_otus (Figure 7B), Shannon (Figure 7C), pielou_e (Figure 7D), dominance (Figure 7E), and Simpson (Figure 7F) did not show significant differences in each group. Compared with the model group, there were significant differences in Chao1 and Observed_otus in the PCP group ($P < 0.05$) and significant differences in pielou_e in the AMX group ($P < 0.05$). There were significant differences in Shannon, pielou_e, and Simpson between the PCP and AMX groups ($P < 0.05$). In the cumulative box plot of species, as shown in Figure 7F, the sample increase rate gradually tended to be flat, indicating that the sample size was sufficient and the results were highly reliable.

Similarly, the obtained ASV feature sequences were analyzed in terms of Beta diversity. Unweighted unifrac distance was used to measure the difference coefficient among the samples, as shown in Figure 8A. The larger the value, the darker the color, indicating the more significant the difference in species diversity among the samples. According to the results of principal coordinate analysis (**PCoA**) (Figure 8B), the first 2 main axes explained 41.26 and 23.65% of the sample variance data. The bray_curtis algorithm was used to compare the species composition of each group, and the results were shown in Figure 8C. Compared with the model group, it had highly significant differences in the blank group, LLP, PCP, and AMX groups ($P < 0.0001$), indicating that using different polysaccharides and drugs had different directions of influence on the differences between groups.

Multivariate Analysis of Untargeted LC/MS Metabolomics

Untargeted serum metabolomic profiles were determined using LC-MS to assess changes in serum metabolites between different groups systematically. After normalization, 8,582 metabolites were obtained. PCA analysis showed that the 6 groups of metabolic differences were statistically significant (PC1 = 36.1, PC2 = 13.3, PC3 = 7.9%) (Figure 9A, B). The result in Figure 9C showed the distribution of all differential metabolites in the 6 groups. Similarly, the ring diagram shown in Figure 9D was used to classify metabolites,

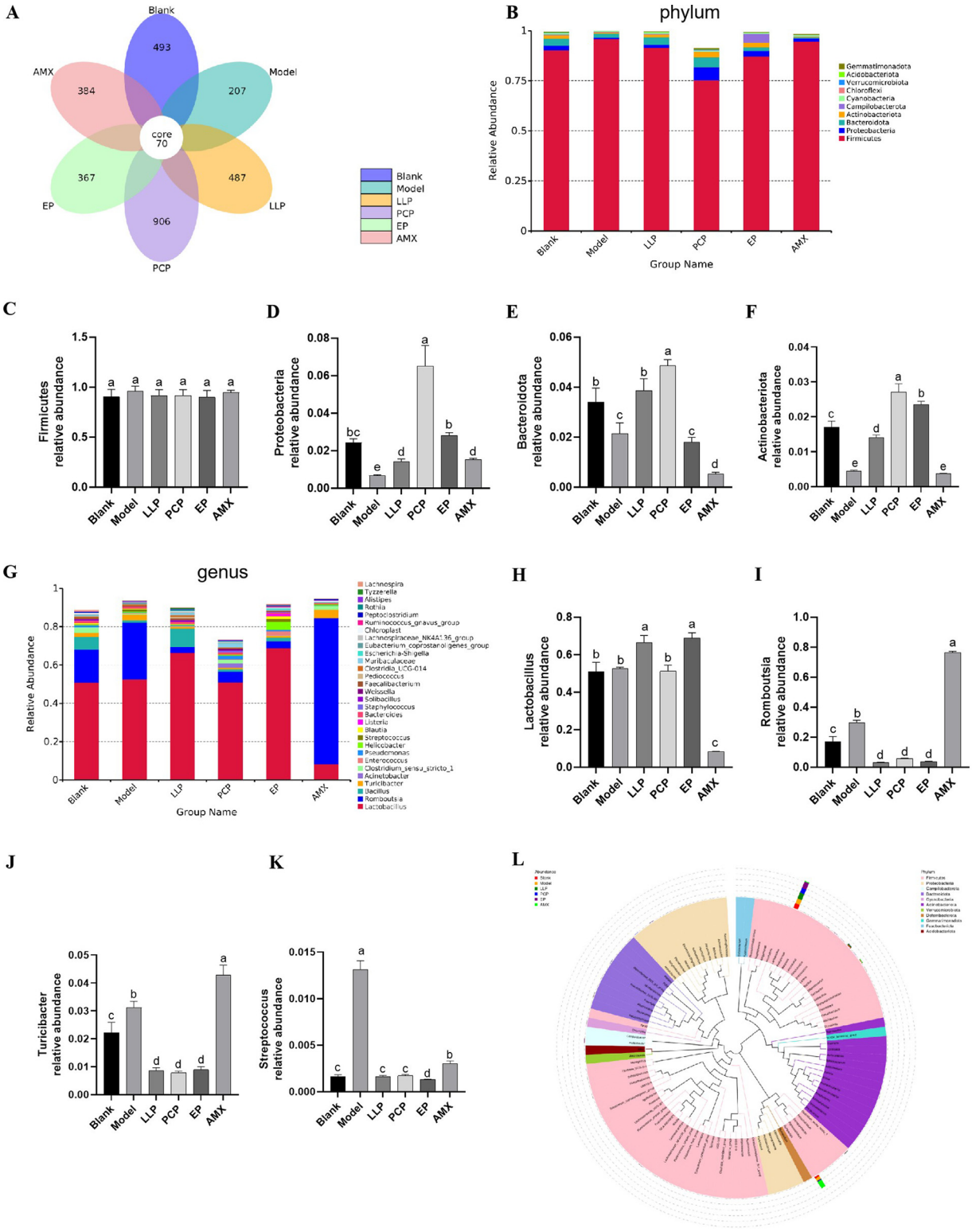

Figure 6. Ileal microbial composition of laying hens. Petal plot of the distribution of ASVs in the 6 groups. Each circle in the figure represents a group, the numbers in the overlapping part of the circle and process represent the number of ASVs shared between groups, and the numbers without overlap represent the number of group-specific ASVs (A), cumulative bar plot of the top 10 species in abundance at Phylum level; The abscissa is grouping; The ordinate represents the relative abundance (B), distribution of Firmicutes in the 6 groups (C), distribution of Proteobacteria in the 6 groups (D), distribution of Bacteroidota in the 6 groups (E), and distribution of ASVs in the 6 groups (C). Distribution of *Actinobacteriota* in the 6 groups (F), a cumulative bar chart of the top 30 species in abundance at the genus level. The abscissa is grouping; the ordinate represents the relative abundance (G), distribution of *Lactobacillus* in the 6 groups (H), distribution of *Romboutsia* in the 6 groups (I), and distribution of *Actinobacteriota* in the 6 groups (F). Distribution of *Turicibacter* in the 6 groups (J), distribution of *Streptococcus* in the 6 groups (K), and the phylogenetic tree of species at the top 100 genus level (L).

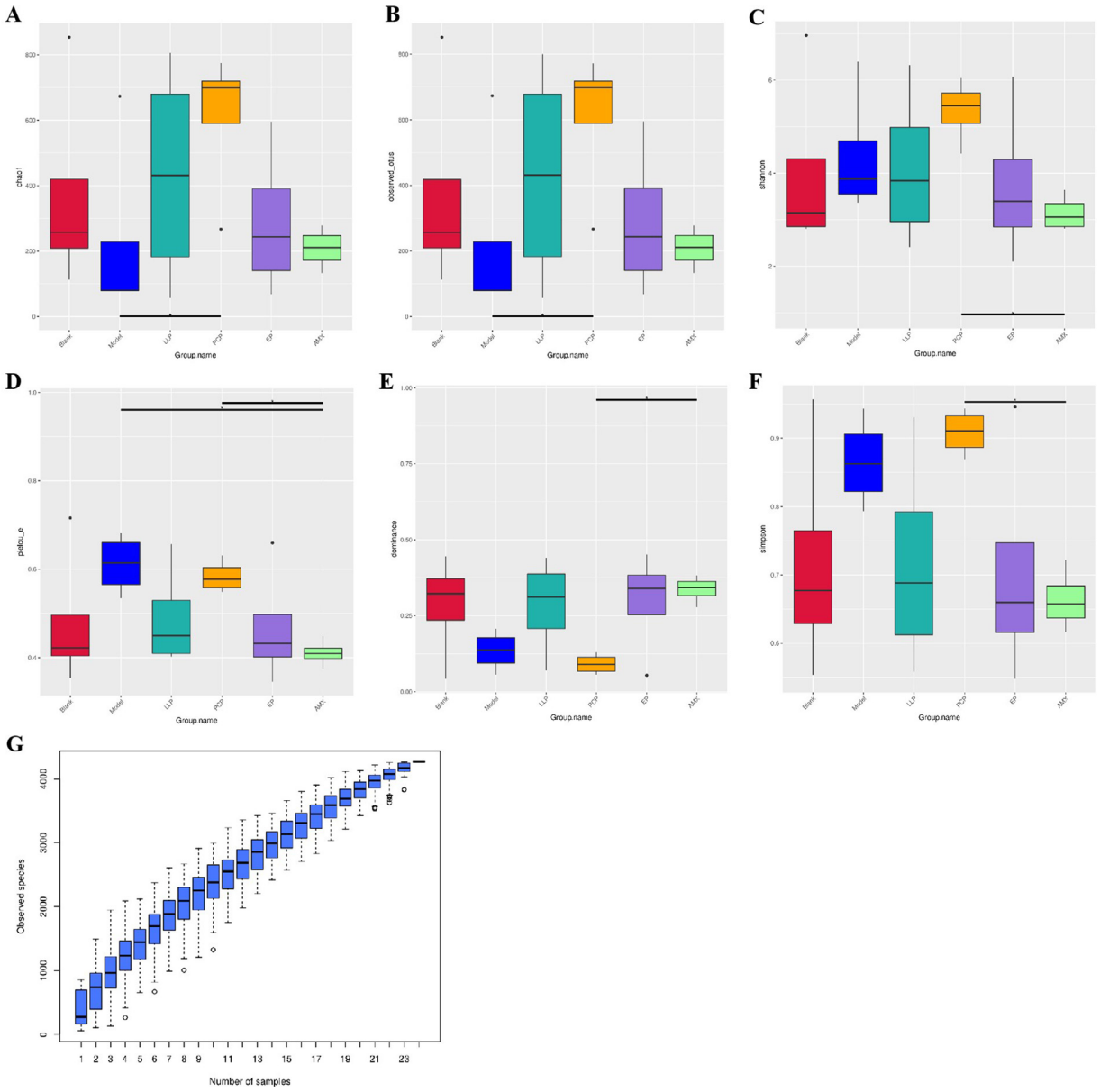

Figure 7. Alpha diversity analysis results. Chao1 index (A), observed_otus index (B), Shannon index (C), pielou_e index (D), dominance index (E) and Simpson index (F), species accumulation box plot (G).

and the results showed that lipids and lipid-like molecules accounted for 40.055%, and organic acids and their derivatives accounted for 22.376%.

To further clarify the differential metabolite changes between different groups, multivariate analysis was conducted based on P value <0.05 of Student t test and variable importance in the projection (**VIP**) >1 of the first principal component of the OPLS-DA model. Five comparison modes, including Blank VS Model, Model VS LLP, Model VS PCP, Model VS EP, and Model VS AMX, were used. The results were shown in Figure 10A to E. There were significant differences in the number of metabolites between different groups. Similarly, to present the change level of common metabolites in other groups more intuitively, the P value of significance was calculated for the quantitative value for each metabolite, and the results were shown in the form of a box plot in Figure 11. A total of 20 metabolites showed different changes between different groups, including 3-hydroxybutyric acid, 4-pyridoxic acid, allantoin, and D-arabitol. Subsequently, the corresponding ratios of the quantitative values of the differential metabolites were calculated by comparing the 6 data groups. Logarithmic transformation was carried out based on 2 for the above results to draw the radar chart, as shown in Figure 12A, to show the corresponding content trends. The results showed that 3-hydroxybutyric acid and isobutyryl-L-carnitine were prominent in the overall metabolite performance. The enrichment results of 6 groups of differential metabolites in KEGG metabolic pathways are shown in Figure 12B. Metabolic pathways, Biosynthesis of amino acids, and ABC transporters were the main signaling pathways in KEGG enrichment analysis.

Finally, the differential metabolites were mapped to KEGG, PubChem, and other authoritative metabolite databases. After the matching information of the

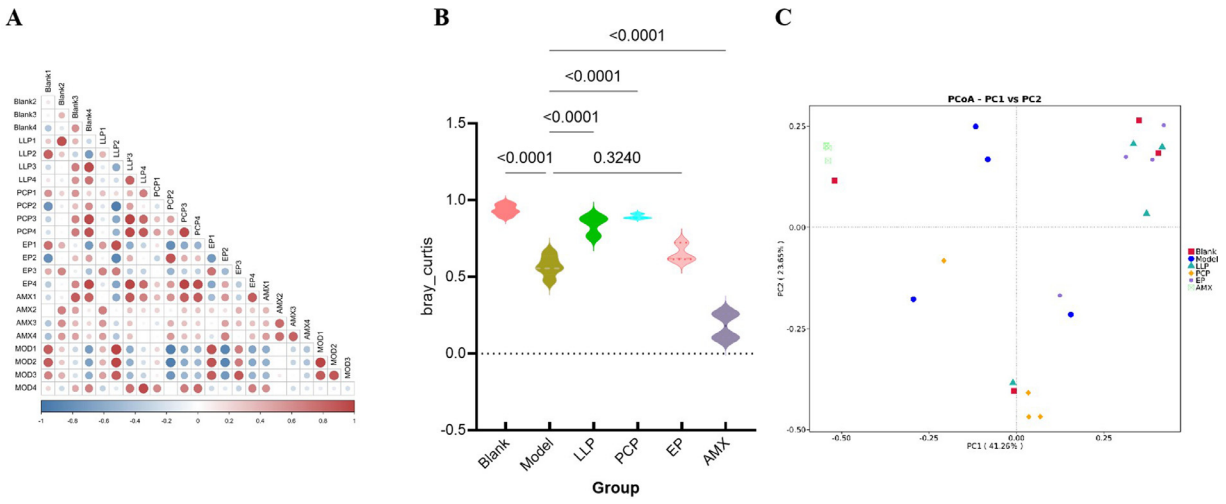

Figure 8. Results of beta diversity analysis. Heat map of the distance matrix, size, and color of circles in squares represents the difference coefficient between 2 samples. The larger the circle, the darker the color, indicating the greater the difference between the 2 samples. Conversely, the smaller the circle, the lighter the corresponding color, meaning that there is less difference between the 2 samples (A), the violin plot of the group difference analysis. The distance algorithm was weighted unifrac distance, the test method was Adonis (B), the PCoA analysis figure. Each point in the figure represents a sample, and points of different colors and shapes distinguish different groups. The percentages in brackets represent the proportion of sample difference data that can be explained by the corresponding axes (C).

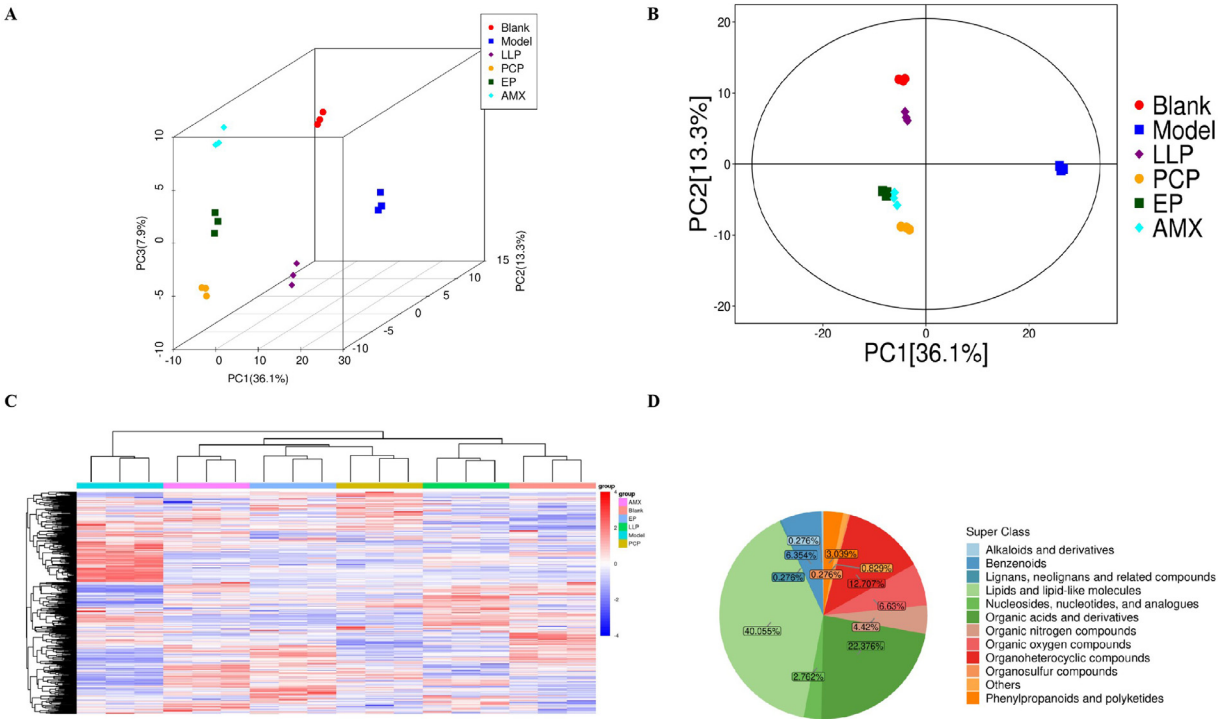

Figure 9. Serum metabolomics results. 3D map of PCA analysis (A), the 2D planar graph of PCA analysis (B), the overall hierarchical clustering analysis heat map of all samples, the abscissa represents different sample groups, the ordinate represents all metabolites, the color blocks at different positions represent the relative expression of metabolites at corresponding positions, and the red represents the high expression of the material content. Blue indicates low expression of the substance (C), ring diagram of metabolite classification and proportion, color blocks indicate different classification categories, and percentage indicates the percentage of metabolites belonging to this type in all identified metabolites (C).

differential metabolites was obtained, the metabolic pathway and regulatory interaction network of the corresponding species *Gallus gallus* (chicken) pathway database were analyzed. The results of metabolic pathways were shown in Figure 13A. There were significant differences in metabolic pathways between the differential metabolites, including Glycine, serine, threonine metabolism, Aminoacyl−tRNA biosynthesis, and beta-alanine metabolism. The regulatory interaction network analysis results were shown in Figure 13B. Twenty-six differential metabolites affected 20 signaling pathways through 32 related regulatory enzymes.

Analysis of Correlation

The analysis results of the correlation analysis between gut microbiota and serum metabolome were shown in a

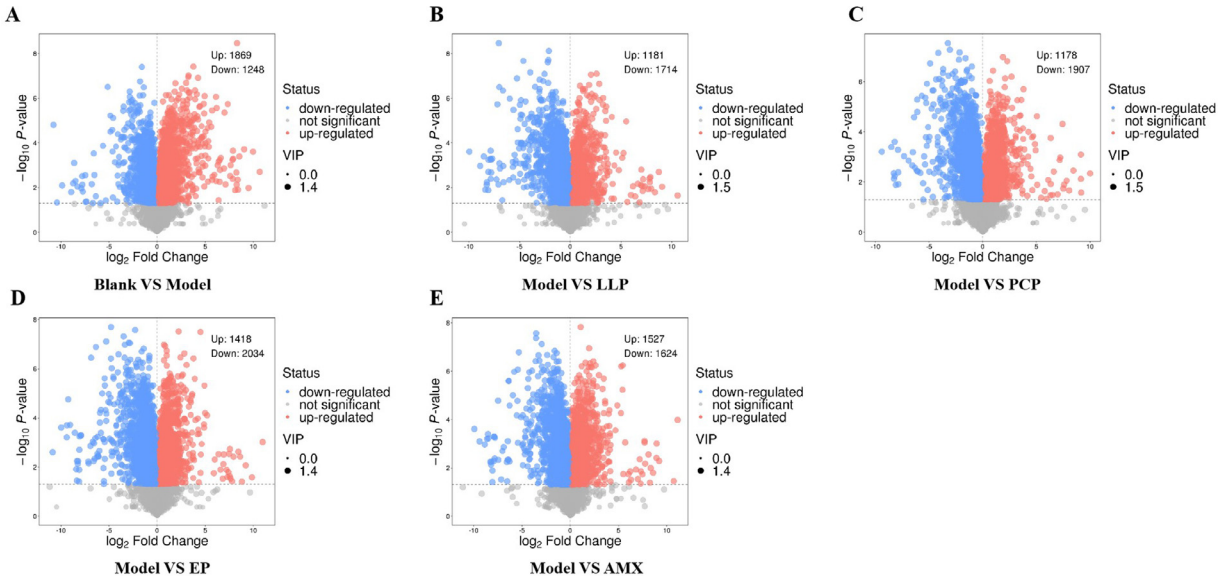

Figure 10. Volcano plot of differential metabolites. Comparison between the blank group and the model group (A), comparison between the model group and the LLP group (B), comparison between the model group and the PCP group (C), comparison between the model group and the EP group (D), comparison between the model group and the AMX group (F). Each point in the volcano plot represents a peak containing all the substances this experiment measured. The horizontal axis represents the fold change of each substance in this group (logarithm base 2), and the vertical axis represents the *P* value of Student *t* test (logarithm base 10 is negative). The size of the scatter points represents the VIP value of the OPLS-DA model, and the larger the scatter points, the larger the VIP value. Significantly upregulated metabolites are shown in red, downregulated considerably in blue, and nonsignificantly different metabolites in gray.

hierarchical clustering heatmap labeled as Figure 14A to E. There were 237 differential metabolites in the blank group compared with the model group and 219, 214, 260, and 249 differential metabolites in the model group compared with LLP, PCP, EP, and AMX groups, respectively. Notably, in comparing the blank and model groups, most metabolites were negatively correlated with *Staphylococcus* and *Helicobacter*. In contrast, *Lactobacillus, Rothia, Turicibacter*, and *Bacillus* were positively correlated between the different polysaccharide groups. This correlation suggested that alterations in the relevant chemicals in serum may be caused by alterations in the gut microbiota of laying hens caused by bacterial infection and polysaccharide feeding.

DISCUSSION

The primary role of the hen ovary is to produce yolk, which falls into the oviduct after maturity. The oviduct is a semiopen pipe for transporting eggs outward and a place for the final formation of eggs (Salas et al., 2017). In this process, inflammation caused by various reasons is the primary resistance to the formation of eggs, and among many conditions, bacterial contamination is the main reason. Salpingitis caused by bacterial infection is a severe poultry disease affecting egg production, including shape, broken, and soft-shell eggs (Yang et al., 2020). This study found that after bacterial challenge, the symptoms of salpingitis were obvious in laying hens, and the number of eggs produced was significantly decreased compared with the blank group, which indicated the feasibility of establishing salpingitis through bacterial infection. However, the number of eggs produced increased in laying hens fed polysaccharides in the early stage, indicating that the effects of TCM and its active ingredients on egg production performance were positively correlated. This result was also confirmed by Liu et al. (Liu et al., 2023a), who reported that egg production and egg quality of laying hens could be further improved after feeding different doses of TCM. The pathological features of salpingitis are a broken oviduct and the appearance of inflammatory secretions. A survey in Jordan pointed out that among 243 hens who died in a specific place, 111 (46%) hens were found to have inflammatory secretions in the body or oviduct tissue, and bacteria such as *Escherichia coli* and *Staphylococcus aureus* were isolated from the autopsy tissue (Jordan et al., 2005). This result also confirmed the pathogenic factor of bacterial infection in salpingitis. Other studies reported inflammatory cell infiltration and thickening and folding of the perifollicular membrane in the pathological tissues of egg-laying hens infected with *E. coli* (Chaudhari and Kariyawasam, 2014). In the present study, oviduct obstruction and white inflammatory secretions were also found in the necropsy of laying hens. Further pathological examination revealed vacuolization of oviduct tissues accompanied by inflammatory cell infiltration in the model group, but these characteristics were improved in the polysaccharide groups.

The colonization and growth of bacteria will destroy the mucosal immune system and cause mucosal inflammation (Buffie and Pamer, 2013). At the same time, eggs without the protection of a shell can provide sufficient nutrients for bacteria, which will cause the body to fall into a vicious cycle, on the one hand, reducing egg production, on the other hand, leading to host infection

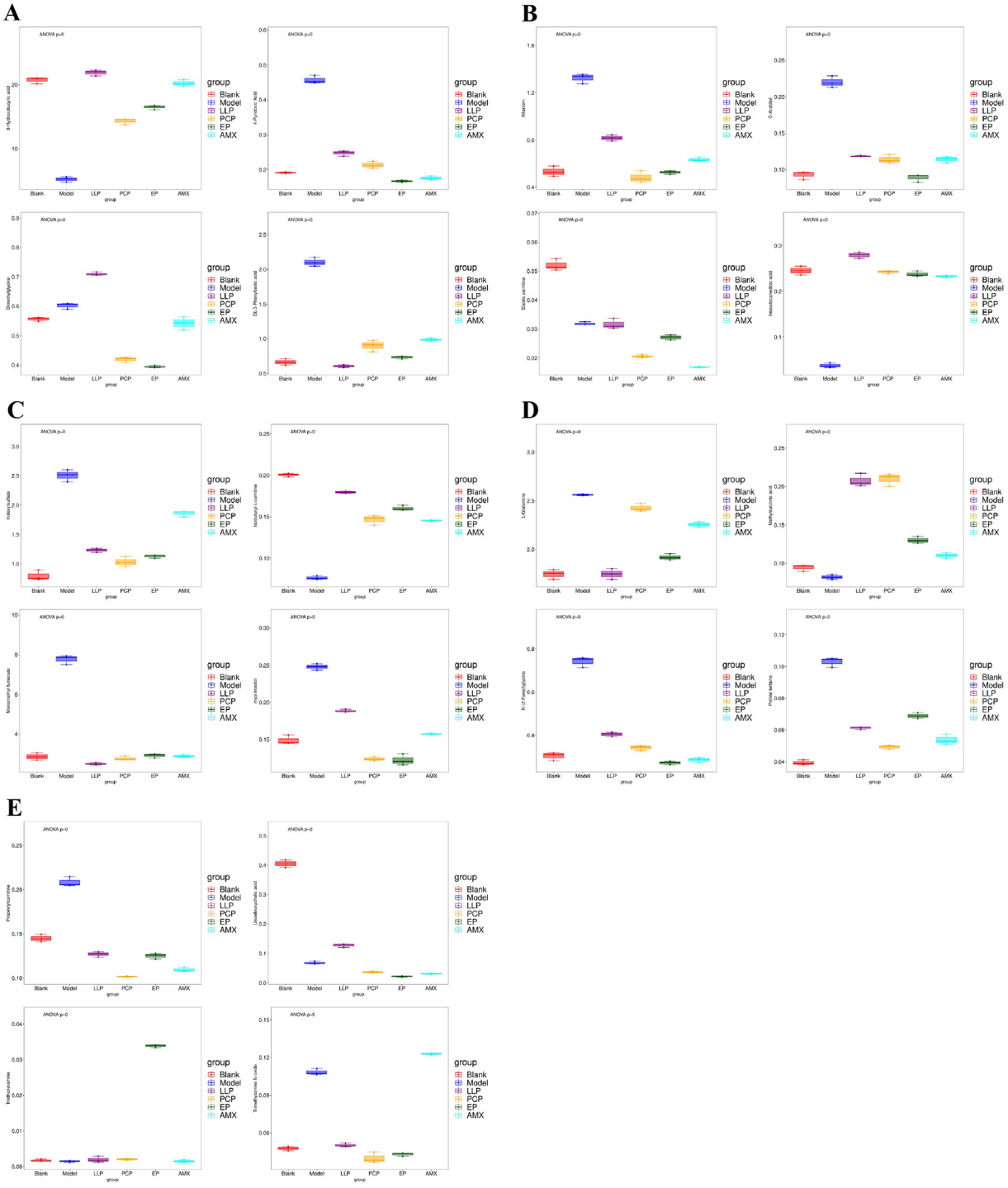

Figure 11. Boxplot of distribution of differential metabolites in 6 groups of samples, the abscissa represents grouping, the ordinate represents content, $P = 0$.

(Liu et al., 2023b). Therefore, mucosal immunity can reflect the immune level of the body to a certain extent. TCM polysaccharides can alleviate the body's inflammatory response caused by bacterial or viral infection and increase the secretion of immunoglobulin in the immune system (Zhu et al., 2018; Shan et al., 2019). IgA and IgM are the first line of defense to protect the mucosal epithelium from toxins and pathogenic microorganisms. IgA can eliminate pathogenic microorganisms by blocking their entry into epithelial receptors, trapping them in mucus, and promoting their clearance through peristalsis and mucociliary activity (Mantis et al., 2011). IgM is the earliest antibody in the primary immune response. In the early stage of bacterial infection, IgM can be rapidly secreted and cleared of pathogens and has bacteriolytic, antibacterial, and neutralizing effects (Boes et al., 1998). In this study, compared with the blank group, the model group showed significant downregulation of IgA and IgM expression after bacterial infection, indicating that mucosal immunity was destroyed. However, this situation was restored after supplementation with different TCM polysaccharides.

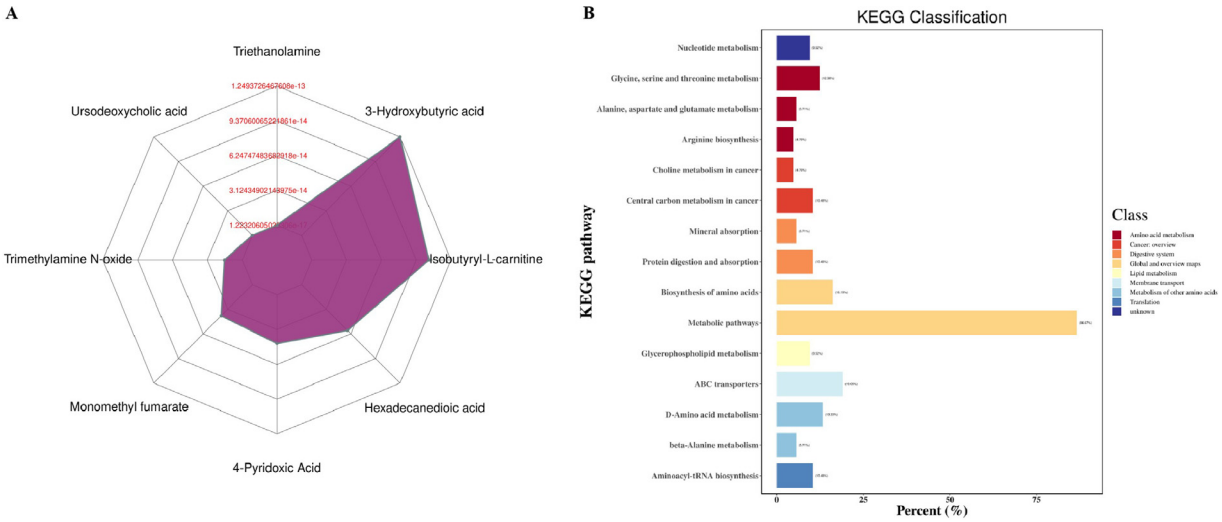

Figure 12. Metabolite trends and KEGG enrichment analysis. Radar map analysis of differential metabolites: the corresponding ratio was calculated for the quantitative values of differential metabolites, and the logarithmic transformation was taken as base 2. The figure is represented by red font, each grid line represents A difference fold, and the purple shade is composed of the line of difference fold for each substance (A). The abscissa represents the percentage of the number of differential metabolites annotated under a specific pathway to the number of all annotated differential metabolites, and the ordinate represents the enriched KEGG metabolic pathway name (B).

Various pharmacological studies have also shown that TCM has antibacterial and immune-enhancing effects (Zhao et al., 2018).

Proinflammatory factors, prominent expression during gram-negative bacterial infection, can induce cells to produce many free radicals, and further lead to the destruction of oxygen-free radical homeostasis in vivo, thereby aggravating oxidative stress (Zhang et al., 2003). MAD and SOD are the core parameters for assessing antioxidant capacity, and GSH is an essential antioxidant for cell survival (Zhong et al., 2023). CAT is a vital antioxidant enzyme that protects against immune infections and oxidative stress (Zhang et al., 2011). TCM polysaccharides have excellent antioxidant activity (Mu et al., 2021). In the present study, the expression level of MDA in the model group was significantly increased after bacterial challenge, accompanied by the decrease of SOD and CAT levels, indicating the activation of oxidative stress response. However, the levels of MDA, SOD, and CAT of laying hens fed with

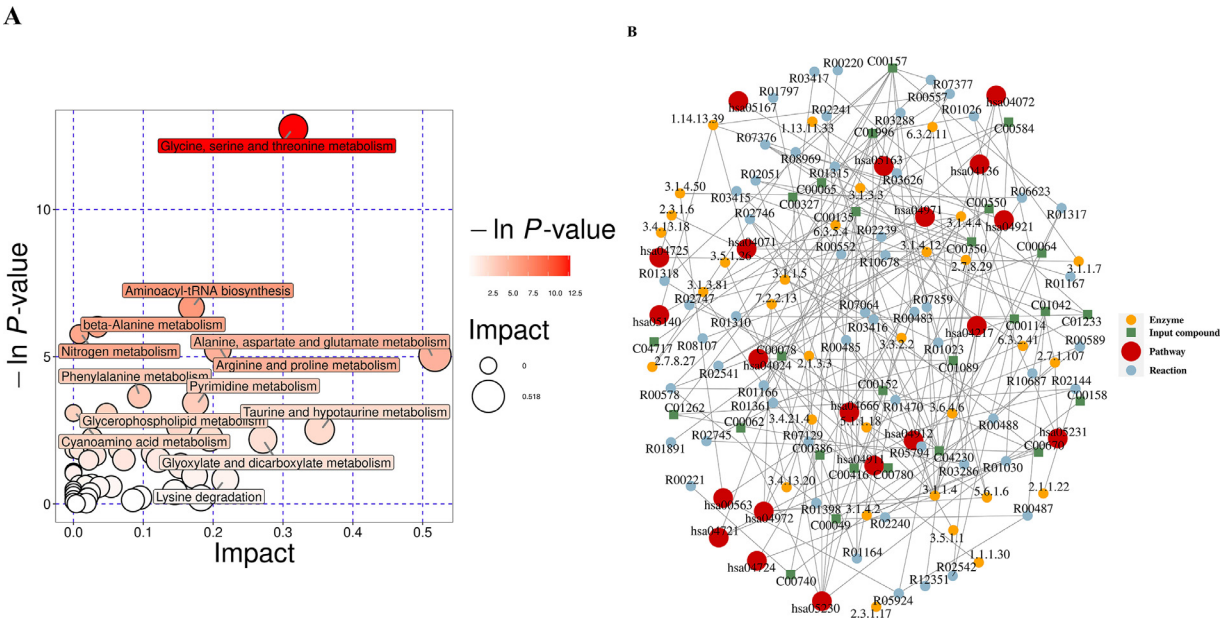

Figure 13. Metabolic pathways and regulatory network analysis. Each bubble in the bubble graph represents a metabolic pathway, and the bubble and size represent the influencing factor of the pathway in the topological analysis. The larger the size, the larger the influencing factor. The bubble's vertical axis and the bubble's color represent the P value of enrichment analysis (taking the negative natural logarithm, namely $-\ln(p)$). The darker the color, the smaller the P value, and the more significant the degree of enrichment (A). In the regulatory network of the differential metabolites, the red dots represent a metabolic pathway, the yellow dots represent substance-related regulatory enzyme information, and the green dots represent the background material of a metabolic pathway. The purple dots represent the molecular module information of a kind of substance, the blue dots represent the chemical interaction of a substance, and the green squares represent the different substances obtained by this comparison (B).

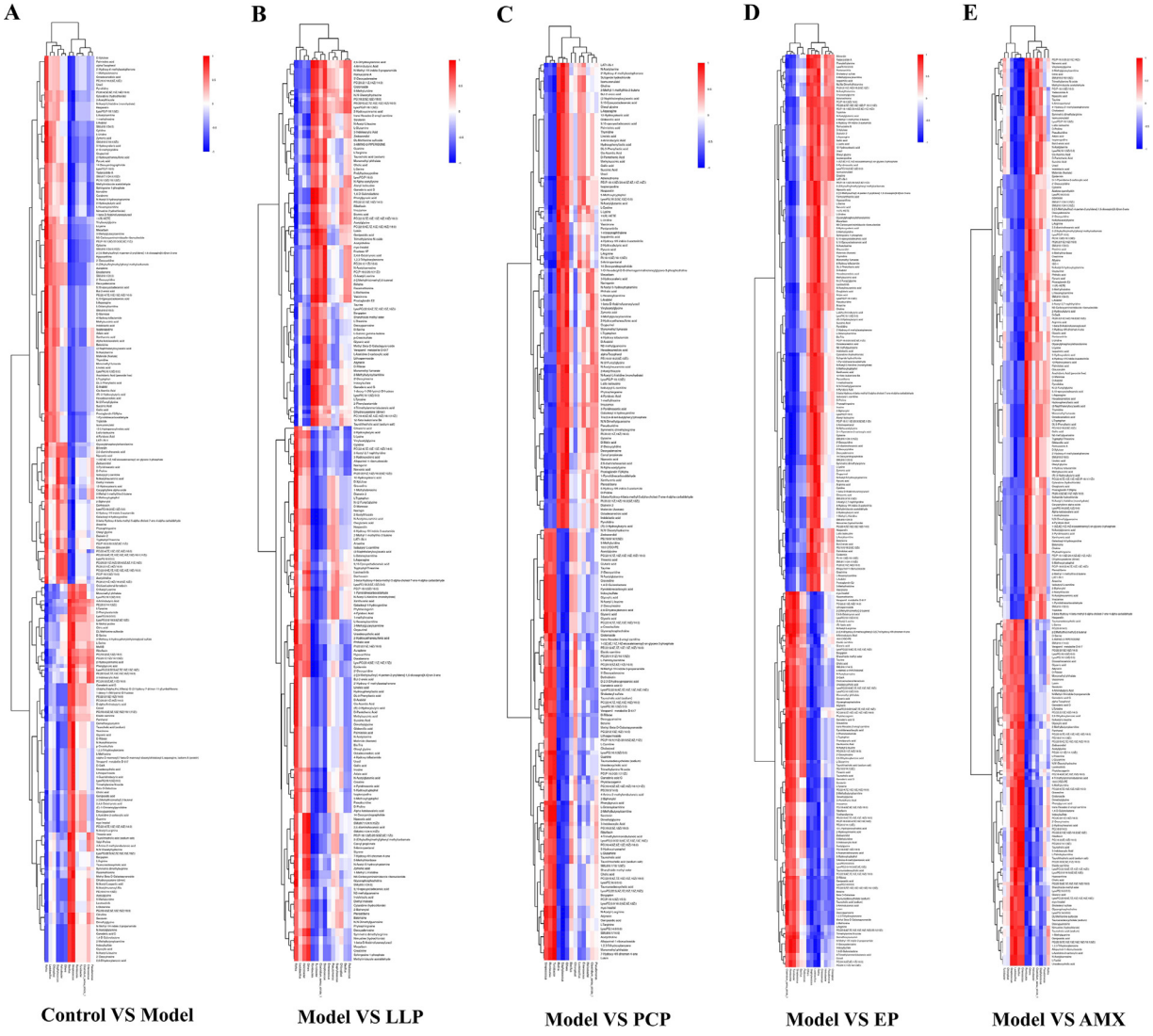

Figure 14. The horizontal and vertical coordinates represent this group's differential metabolites and flora. The color blocks at different positions represent the correlation coefficient between the metabolites and the flora at the corresponding positions. The red represents the positive correlation; the blue represents the negative correlation, and the darker the color represents, the stronger the correlation. A significant correlation is marked with "*" ($P < 0.05$). The clustering results are presented as a dendrogram on the side of the heat map, expressing the quantity phase of a cluster of metabolic substances or bacteria.

polysaccharides in advance were significantly different from those of the model group after bacterial challenge, and this good regulation indicated that the antioxidative stress of the polysaccharide group was improved.

Gram-negative bacteria release large amounts of endotoxins (such as LPS) during the reproduction and growth of infected hosts (Park and Lee, 2013). LPS-binding protein LBP can recognize it and bind to mCD14 on the surface of myeloid cells to form the LPS-LBP-CD14 triple complex, which binds to TLR4 with the help of MD-2. TLR4 is activated and dimerized. Upon activation, TLR4 transmits signals into the cell to recruit MyD88 and subsequently activates the NFκB/MAPK signaling pathway, which promotes the release of TNF-α, IL1, and IL6 (Kayagaki et al., 2013). Then, the signal transduction pathway will continue activating monocytes, macrophages, endothelial cells, and epithelial cells to synthesize and release various cytokines and inflammatory mediators, causing inflammatory responses (Zhao et al., 2021). IFN-γ released by activated T cells and NK cells can further aggravate the inflammatory response. Notably, IFN-γ plays an essential role in innate and adaptive immunity against viral, certain bacterial, and protozoan infections, and it can also activate macrophages and induce their release of IL8 (Zhang et al., 2017). IL5, secreted by Th2 cells and mast cells, can stimulate IgA and IgM production (Takatsu et al., 1988). Studies have shown that IL5 can regulate various inflammatory responses and promote the rapid clearance of pathogens (Dougan et al., 2019). In the present study, the TLR4/NFκB signaling pathway was activated in the oviduct tissue of the model group compared with the blank group after bacterial challenge. At the same time, the mRNA expression levels of TNF-α, IFN-γ, IL1β, IL6, and IL8 were significantly increased, while the mRNA expression level of IL5 was decreased considerably. The results showed that an inflammatory response was produced in laying hens, which was consistent with the IgA and IgM findings. After prefeeding the polysaccharide, the mRNA

expression of the TLR4/NFκB signaling pathway and proinflammatory factors was downregulated, and the mRNA expression of IL5 was increased in the polysaccharide group. The anti-inflammatory effect of polysaccharides was further confirmed.

The composition of gut microbiota is under the surveillance of the normal mucosal immune system, and inflammation is caused by the abnormal immune response, which can affect the balance of gut microbiota (Shi et al., 2017). There is a link between gut microbiota and disease progression. As mentioned above, the intake of polysaccharides can improve the composition of gut microbiota, which has also been confirmed in several studies (Cui et al., 2021; Cao et al., 2023). *Firmicutes* and *Proteobacteria* were shown to be the most abundant bacterial taxa in chicken ileum contents (Alvarenga et al., 2023). Many members of the phylum *Firmicutes* are beneficial and core-dominant bacteria in humans and animals. Proteobacteriade dysregulation (increased or decreased) can lead to bacterial enteritis (Martin-Nuñez et al., 2021). However, some studies have found that the presence of *Proteobacteria* may benefit the body. For example, the specific regulation of IgA promotes gut microbial maturation (Mirpuri et al., 2014). In this study, bacterial infection and polysaccharide feeding did not affect *Firmicutes* abundance. However, the abundance of *Proteobacteriade* was decreased in the model and the AMX groups, indicating that the intestinal microbiota in these 2 groups may be disordered. Although *Proteobacteriade* increased in the PCP group, it did not affect the previous anti-inflammatory performance, which may be related to the beneficial effect of PCP. *Bacteroidetes* and *Actinobacteria* are also resident bacteria in laying hens' gut (Dai et al., 2022). *Bacteroidetes* participate in many important metabolic activities in the intestinal tract, including carbohydrate fermentation, bile acid, and other steroid fermentation (Brinkmann et al., 2022). It has been shown that polysaccharides from plants are the main energy source of *Bacteroides*, so feeding polysaccharides can promote the proliferation of *Bacteroides* (Zafar and Saier, 2021). *Actinobacteria* play an important role in the turnover of organic matter and carbon cycle, such as decomposing cellulose (Wang et al., 2023). At the same time, the beneficial bacteria of *Actinobacteria* often help the body to improve digestive problems and enhance immunity (Xiao et al., 2020). In the present study, the significant downregulation of *Bacteroidetes* and *Actinobacteria* in the model group further explained the disturbance of the gut microbiota of laying hens. Both bacteria were relatively restored after polysaccharide supplementation, indicating that feeding polysaccharides can promote the colonization and growth of beneficial bacteria in the intestine. Notably, both of the above bacteria were significantly decreased in the AMX group. This result was believed to be inseparable from the disruption of intestinal microbial balance by antibiotics (Zeng et al., 2023). *Lactobacillus* is a group of gram-positive bacteria belonging to the *Lactobacillus Firmicutes* family. It has a variety of functions, including maintaining the balance of flora, improving digestion, and enhancing immunity. It had been reported that *Lactobacilli* isolated from chickens had the same antibacterial ability (Dec et al., 2016) and improved the ability to prevent infectious diseases and the performance of chickens (Benbara et al., 2020). Growing evidence showed that an increased abundance of *Romboutsia* was associated with inflammatory diseases. *Clostridium_sensu_stricto_1* and *Romboutsia* were significantly upregulated in alcohol-induced liver injury in mice (Zhang et al., 2023), as well as in mice with dextran sulfate-induced colitis. The abundance of *Romboutsia* was also increased after cephalosporin treatment (Wang et al., 2022). *Turicibacter* is an enteric pathogen. It has been reported that the abundance of *Turicibacter* was significantly increased in necrotic enteritis (**NE**)-induced chicken intestines and decreased after astragalus polysaccharide (**APS**) supplementation (Song et al., 2022). A high expression of *Turicibacter* was similarly found in the gut of DSS-induced colitis in mice reported by Zhang et al., and a downward trend in the abundance of this bacterium was also observed after icariin feeding (Zhang et al., 2021). The genus *Streptococcus* is the cause of millions of cases of meningitis, bacterial pneumonia, endocarditis, erysipelas, and necrotizing fasciitis (Ge and Sun, 2014). It is one of the main harmful bacteria that can inhibit the growth of chickens (Houghton and Fuller, 1980). In this study, the abundance of *Lactobacillus* increased after LLP and EP supplementation and significantly decreased in the AMX group. *Romboutsia, Turicibacter*, and *Streptococcus* increased abundance in the model and AMX groups but decreased in the polysaccharide groups. These results suggested that feeding polysaccharides could significantly increase the abundance of beneficial bacteria and reduce the abundance of harmful bacteria in laying hens. Although antibiotics could reduce the abundance of streptococcal bacteria to a certain extent, they also cause intestinal flora disturbance.

The metabolic and immune systems are the most basic conditions for the body's survival. Many metabolic and immune responses or pathogen infections are inextricably linked (Hotamisligil, 2006). In the present study, 3,117 differential metabolites were found between the blank and bacteria-infected layers, which further indicated that bacterial infection was also closely related to metabolism. Studies also have shown that plant polysaccharides could regulate metabolic disorders in the body (Li et al., 2021). Liu et al. found that in a model of florfenicol (**FFC**)-induced hepatic metabolic disorder in chicks, feeding *Salvia miltiorrhiza* polysaccharide alleviated the situation through drug metabolism and P450 signaling pathways (Liu et al., 2022). 3-Hydroxybutyric acid, an organic acid ketone body and endogenous product of fatty acid oxidation is the core metabolite of anti-aging, which can inhibit oxidative stress by changing the genes encoding FOXO3A and MT2 (Møller, 2020). In addition, it can reduce the pathological progression of Alzheimer's disease by inhibiting the activation of NLRP3 inflammasome (Shippy et al., 2020). Also, 3-

hydroxybutyric acid alleviated inflammatory progression in DSS-induced colitis mice by promoting the STAT2 signaling pathway and M6 macrophage polarization (Huang et al., 2022). Other studies have shown that 3-hydroxybutyric acid could be produced by some beneficial bacteria and used to treat enteritis (Yan et al., 2021). Hexadecanedioic acid is a product of nonmetabolizing long-chain fatty acids and induces the proliferation of liver peroxidase to improve the body's antioxidant capacity (Hertz et al., 1988). At the same time, it has a significant cholesterol-lowering effect (Mayorek and Bar-Tana, 1993). Some studies have shown that adding hexadecanedioic acid into the diet could reduce the content of unsaturated fatty acids in egg yolk and alter fatty acid metabolism in the liver of laying hens (Elkin et al., 1992). Methylsuccinic acid is a metabolic marker in patients with isovaleric acidemia (De Biase et al., 2019). Studies have shown that methylsuccinic acid could cause the highest upregulation of endothelial nitric oxide synthase expression at the protein level, possibly leading to endothelial cell injury (Lincha et al., 2016). Similarly, methylsuccinic acid was also found in the serum of hyperlipidemic rats (Huang et al., 2021). In this study, 20 metabolites, including 3-hydroxybutyric acid, hexadecanedioic acid, and methylsuccinic acid, showed different trends in 6 groups of samples. 3-Hydroxybutyric acid and Hexadecanedioic acid were downregulated in the model group and increased in the polysaccharide groups. However, the content of methylsuccinic acid was increased in the model group and decreased in the polysaccharide groups. Notably, 3-hydroxybutyric acid was the most prominent compound in the subsequent phenotypic radar map analysis. Then, the combined analysis results with the microbiome showed that 3-hydroxybutyric acid and beneficial bacteria such as *Rhosia* showed a significant positive relationship. However, there was a significant negative relationship with pathogens such as *Romboutsia*. These data suggested that supplementation with TCM polysaccharides could modulate the metabolome of bacteria-induced salpingitis laying hens, which may be closely linked to changes in gut microbes.

CONCLUSIONS

In this study, it was found that supplementation of TCM polysaccharides could further alleviate the bacteria-induced salpingitis of laying hens, improve the antioxidant and immune levels, reduce the mRNA expression levels of inflammation-related cytokines, and increase the egg production of laying hens by regulating the intestinal microbiome and metabolism. The results will provide a theoretical basis for the use of TCM polysaccharides in breeding laying hens.

ACKNOWLEDGMENTS

This research was supported by the Engineering Research Center of Ecology and Agricultural Use of Wetland, Ministry of Education (KFT202306), Jingzhou 2022 Natural Science Research Project (202254-07CC), and the Unveiling Project of "Construction of Advanced Technology Integration Demonstration Base and Targeted Research" in Shishou County (SS202311).

DISCLOSURES

No conflict of interest exists in submitting this manuscript, and all authors approve the manuscript for publication. I want to declare on behalf of my coauthors that the work described was original research that has not been published previously and is not under consideration for publication elsewhere, in whole or in part. All the authors listed have approved the manuscript that is enclosed.

REFERENCES

Alvarenga, B. O., J. B. Paiva, A. I. S. Souza, D. R. Rodrigues, P. C. Tizioto, and A. J. P. Ferreira. 2023. Metagenomics analysis of the morphological aspects and bacterial composition of broiler feces. Poult. Sci. 102:102401.

Bacanlı, M., and N. Başaran. 2019. Importance of antibiotic residues in animal food. Food Chem. Toxicol. 125:462–466.

Benbara, T., S. Lalouche, D. Drider, and F. Bendali. 2020. Lactobacillus plantarum S27 from chicken faeces as a potential probiotic to replace antibiotics: in vivo evidence. Benef. Microbes 11:163–173.

Bisgaard, M. 1995. Salpingitis in web-footed birds: prevalence, aetiology and significance. Avian Pathol. 24:443–452.

Boes, M., A. P. Prodeus, T. Schmidt, M. C. Carroll, and J. Chen. 1998. A critical role of natural immunoglobulin M in immediate defense against systemic bacterial infection. J. Exp. Med. 188:2381–2386.

Bonfante, F., E. Mazzetto, C. Zanardello, A. Fortin, F. Gobbo, S. Maniero, M. Bigolaro, I. Davidson, R. Haddas, G. Cattoli, and C. Terregino. 2018. A G1-lineage H9N2 virus with oviduct tropism causes chronic pathological changes in the infundibulum and a long-lasting drop in egg production. Vet. Res. 49:83.

Brinkmann, S., M. S. Spohn, and T. F. Schäberle. 2022. Bioactive natural products from Bacteroidetes. Nat. Prod. Rep. 39:1045–1065.

Buffie, C. G., and E. G. Pamer. 2013. Microbiota-mediated colonization resistance against intestinal pathogens. Nat. Rev. Immunol. 13:790–801.

Cao, Z., Z. Liu, N. Zhang, C. Bao, X. Li, M. Liu, W. Yuan, H. Wu, and H. Shang. 2023. Effects of dietary dandelion (Taraxacum mongolicum Hand.-Mazz.) polysaccharides on the performance and gut microbiota of laying hens. Int. J. Biol. Macromol. 240:124422.

Chaudhari, A. A., and S. Kariyawasam. 2014. An experimental infection model for Escherichia coli egg peritonitis in layer chickens. Avian Dis. 58:25–33.

Cheng, H., S. Feng, X. Jia, Q. Li, Y. Zhou, and C. Ding. 2013. Structural characterization and antioxidant activities of polysaccharides extracted from Epimedium acuminatum. Carbohydr. Polym. 92:63–68.

Cheng, L., W. Zhang, Q. Jin, Y. Zhu, R. Chen, Q. Tian, N. Yan, and L. Guo. 2021. The effects of dietary supplementation with lotus leaf extract on the immune response and intestinal microbiota composition of broiler chickens. Poult. Sci. 100:100925.

Cui, L., X. Guan, W. Ding, Y. Luo, W. Wang, W. Bu, J. Song, X. Tan, E. Sun, Q. Ning, G. Liu, X. Jia, and L. Feng. 2021. Scutellaria baicalensis Georgi polysaccharide ameliorates DSS-induced ulcerative colitis by improving intestinal barrier function and modulating gut microbiota. Int. J. Biol. Macromol. 166:1035–1045.

Dai, D., G.-H. Qi, J. Wang, H.-J. Zhang, K. Qiu, and S.-G. Wu. 2022. Intestinal microbiota of layer hens and its association with egg quality and safety. Poult. Sci. 101:102008.

De Biase, I., M. Pasquali, and A. Asamoah. 2019. Unusual metabolites in a patient with isovaleric acidemia. Clin. Chem. 65:595–597.

Dec, M., A. Puchalski, A. Nowaczek, and A. Wernicki. 2016. Antimicrobial activity of Lactobacillus strains of chicken origin against bacterial pathogenss. Int. Microbiol. 19:57–67.
Dougan, M., G. Dranoff, and S. K. Dougan. 2019. GM-CSF, IL-3, and IL-5 family of cytokines: regulators of inflammation. Immunity 50:796–811.
Elkin, R. G., J. C. Rogler, H. D. Lee, and B. A. Watkins. 1992. Effect of beta, beta'-tetramethyl-substituted hexadecanedioic acid (MEDICA 16) on laying hen performance and egg yolk lipid composition. Br. Poult. Sci. 33:677–681.
Fang, H., H. Quan, Y. Zhang, Q. Li, Y. Wang, S. Yuan, S. Huang, and C. He. 2021. Co-infection of Escherichia coli, Enterococcus faecalis and Chlamydia psittaci contributes to salpingitis of laying layers and breeder ducks. Pathogens 10:755.
Ge, R., and X. Sun. 2014. Iron acquisition and regulation systems in Streptococcus species. Metallomics 6:996–1003.
Guo, L., J. Liu, Y. Hu, D. Wang, Z. Li, J. Zhang, T. Qin, X. Liu, C. Liu, X. Zhao, Y. P. Fan, G. Han, and T. L. Nguyen. 2012. Astragalus polysaccharide and sulfated Epimedium polysaccharide synergistically resist the immunosuppression. Carbohydr. Polym. 90:1055–1060.
Hertz, R., J. Bar-Tana, M. Sujatta, J. Pill, F. H. Schmidt, and H. D. Fahimi. 1988. The induction of liver peroxisomal proliferation by beta,beta'-methyl-substituted hexadecanedioic acid (MEDICA 16). Biochem. Pharmacol. 37:3571–3577.
Hotamisligil, G. S. 2006. Inflammation and metabolic disorders. Nature 444:860–867.
Houghton, S. B., and R. Fuller. 1980. Ecology of Streptococcus faecium bacteriophage in chicken gut. Appl. Environ. Microbiol. 39:1054–1058.
Huang, C., J. Wang, H. Liu, R. Huang, X. Yan, M. Song, G. Tan, and F. Zhi. 2022. Ketone body β-hydroxybutyrate ameliorates colitis by promoting M2 macrophage polarization through the STAT6-dependent signaling pathway. BMC Med. 20:148.
Huang, J., N. Xiao, Y. Sun, S. Wu, W. Tian, Y. Lai, P. Li, and B. Du. 2021. Supplementation of Bacillus sp. DU-106 reduces hypercholesterolemia and ameliorates gut dysbiosis in high-fat diet rats. Appl. Microbiol. Biotechnol. 105:287–299.
Johnson, T. J., C. Fernandez-Alarcon, A. M. Bojesen, L. K. Nolan, D. W. Trampel, and T. Seemann. 2011. Complete genome sequence of Gallibacterium anatis strain UMN179, isolated from a laying hen with peritonitis. J. Bacteriol. 193:3676–3677.
Jordan, F. T. W., N. J. Williams, A. Wattret, and T. Jones. 2005. Observations on salpingitis, peritonitis and salpingoperitonitis in a layer breeder flock. Vet. Rec. 157:573–577.
Kayagaki, N., M. T. Wong, I. B. Stowe, S. R. Ramani, L. C. Gonzalez, S. Akashi-Takamura, K. Miyake, J. Zhang, W. P. Lee, A. Muszyński, L. S. Forsberg, R. W. Carlson, and V. M. Dixit. 2013. Noncanonical inflammasome activation by intracellular LPS independent of TLR4. Science 341:1246–1249.
Li, T.-T., Z.-R. Huang, R.-B. Jia, X.-C. Lv, C. Zhao, and B. Liu. 2021. Spirulina platensis polysaccharides attenuate lipid and carbohydrate metabolism disorder in high-sucrose and high-fat diet-fed rats in association with intestinal microbiota. Food Res. Int. 147:110530.
Lincha, V. R., B.-T. Zhao, M.-H. Woo, I.-J. Yang, and H.-M. Shin. 2016. Effects of constituent compounds of smilax China on nicotine-induced endothelial dysfunction in human umbilical vein endothelial cells. Biol. Pharm. Bull. 39:984–992.
Liu, Z. P., J. R. Chao, P. T. Xu, H. Y. Lv, B. Y. Ding, Z. F. Zhang, L. L. Li, and S. S. Guo. 2023b. Lonicera flos and Cnicus japonicus extracts improved egg quality partly by modulating antioxidant status, inflammatory-related cytokines and shell matrix protein expression of oviduct in laying hens. Poult. Sci. 102:102561.
Liu, W., Y. Liu, S. Fang, W. Yao, X. Wang, Y. Bao, and W. Shi. 2022. Salvia miltiorrhiza polysaccharides alleviates florfenicol-induced liver metabolic disorder in chicks by regulating drug and amino acid metabolic signaling pathways. Poult. Sci. 101:101989.
Liu, B., R. Ma, Q. Yang, Y. Yang, Y. Fang, Z. Sun, and D. Song. 2023a. Effects of traditional chinese herbal feed additive on production performance, egg quality, antioxidant capacity, immunity and intestinal health of laying hens. Animals (Basel) 13:2510.
Mantis, N. J., N. Rol, and B. Corthésy. 2011. Secretory IgA's complex roles in immunity and mucosal homeostasis in the gut. Mucosal Immunol. 4:603–611.
Martin-Nuñez, G. M., I. Cornejo-Pareja, M. Clemente-Postigo, and F. J. Tinahones. 2021. Gut microbiota: the missing link between *Helicobacter pylori* infection and metabolic disorders? Front. Endocrinol. (Lausanne) 12:639856.
Mayorek, N., and J. Bar-Tana. 1993. Hypocholesterolaemic effect of beta beta'-methyl-substituted hexadecanedioic acid (MEDICA 16) in the male hamster. Biochem. J. 289(Pt 3):911–917.
Mirpuri, J., M. Raetz, C. R. Sturge, C. L. Wilhelm, A. Benson, R. C. Savani, L. V. Hooper, and F. Yarovinsky. 2014. Proteobacteria-specific IgA regulates maturation of the intestinal microbiota. Gut Microbes 5:28–39.
Møller, N. 2020. Ketone body, 3-hydroxybutyrate: minor metabolite - major medical manifestations. J. Clin. Endocrinol. Metab. 105.
Mu, S., W. Yang, and G. Huang. 2021. Antioxidant activities and mechanisms of polysaccharides. Chem. Biol. Drug Des. 97:628–632.
Park, B. S., and J.-O. Lee. 2013. Recognition of lipopolysaccharide pattern by TLR4 complexes. Exp. Mol. Med. 45:e66.
Pors, S. E., R. H. Olsen, and J. P. Christensen. 2014. Variations in virulence of avian pathogenic Escherichia coli demonstrated by the use of a new in vivo infection model. Vet. Microbiol. 170:368–374.
Rasouli, M., A. Ostovar-Ravari, and H. Shokri-Afra. 2014. Characterization and improvement of phenol-sulfuric acid microassay for glucose-based glycogen. Eur. Rev. Med. Pharmacol. Sci. 18:2020–2024.
Salas, C., R. D. Ekmay, J. A. England, S. Cerrate, and C. N. Coon. 2017. Mechanisms of lipid mobilization towards egg formation in broiler breeder hens using stable isotopes. Poult. Sci. 96:383–387.
Shalaby, A. A., R. D. Slemons, and D. E. Swayne. 1994. Pathological studies of A/chicken/Alabama/7395/75 (H4N8) influenza virus in specific-pathogen-free laying hens. Avian Dis. 38:22–32.
Shan, C., B. Sun, R. A. Dalloul, Z. Zhai, P. Sun, M. Li, S. Yang, and W. Luan. 2019. Effect of the oral administration of astragalus polysaccharides on jejunum mucosal immunity in chickens vaccinated against Newcastle disease. Microb. Pathog. 135:103621.
Shi, N., N. Li, X. Duan, and H. Niu. 2017. Interaction between the gut microbiome and mucosal immune system. Mil Med. Res. 4:14.
Shippy, D. C., C. Wilhelm, P. A. Viharkumar, T. J. Raife, and T. K. Ulland. 2020. β-Hydroxybutyrate inhibits inflammasome activation to attenuate Alzheimer's disease pathology. J. Neuroinflamm. 17:280.
Song, B., P. Li, S. Yan, Y. Liu, M. Gao, H. Lv, Z. Lv, and Y. Guo. 2022. Effects of dietary Astragalus polysaccharide supplementation on the Th17/Treg balance and the gut microbiota of broiler chickens challenged with necrotic enteritis. Front. Immunol. 13:781934.
Sun, Y., F. Wang, Y. Liu, S. Liu, Y. An, H. Xue, J. Wang, F. Xia, X. Chen, and Y. Cao. 2022. Microbiome-metabolome responses of Fuzhuan brick tea crude polysaccharides with immune-protective benefit in cyclophosphamide-induced immunosuppressive mice. Food Res. Int. 157:111370.
Takatsu, K., A. Tominaga, N. Harada, S. Mita, M. Matsumoto, T. Takahashi, Y. Kikuchi, and N. Yamaguchi. 1988. T cell-replacing factor (TRF)/interleukin 5 (IL-5): molecular and functional properties. Immunol. Rev. 102:107–135.
Tian, H., Z. Liu, Y. Pu, and Y. Bao. 2019. Immunomodulatory effects exerted by Poria cocos polysaccharides via TLR4/TRAF6/NF-κB signaling in vitro and in vivo. Biomed. Pharmacother. 112:108709.
Walsh, T. R., and Y. Wu. 2016. China bans colistin as a feed additive for animals. Lancet Infect. Dis. 16:1102–1103.
Wang, C., L. Feng, J. Su, L. Cui, L. Dan, J. Yan, C. Ding, X. Tan, and X. Jia. 2017. Polysaccharides from Epimedium koreanum Nakai with immunomodulatory activity and inhibitory effect on tumor growth in LLC-bearing mice. J. Ethnopharmacol. 207:8–18.
Wang, C., S. E. Pors, J. P. Christensen, A. M. Bojesen, and I. Thøfner. 2020. Comparison and assessment of necropsy lesions in end-of-lay laying hens from different housing systems in Denmark. Poult. Sci. 99:119–128.
Wang, X., M. Yu, X. He, J. Su, B. Xi, Y. Sun, X. Fu, Y. Wang, and M. Zheng. 2023. Insights into the role of the microbial community lifestyle strategies in variations of the dissolved organic matter molecular composition along an effluent-dominated river. Chemosphere 310:136829.
Wang, H.-G., M.-N. Zhang, X. Wen, L. He, M.-H. Zhang, J.-L. Zhang, and X.-Z. Yang. 2022. Cepharanthine ameliorates dextran

sulphate sodium-induced colitis through modulating gut microbiota. Microb. Biotechnol. 15:2208–2222.

Wu, D.-T., K.-L. Feng, F. Li, Y.-C. Hu, S.-P. Wang, R.-Y. Gan, and L. Zou. 2022. In vitro digestive characteristics and microbial degradation of polysaccharides from lotus leaves and related effects on the modulation of intestinal microbiota. Curr. Res. Food Sci. 5:752–762.

Xiao, Y., J. Zhao, H. Zhang, Q. Zhai, and W. Chen. 2020. Mining Lactobacillus and Bifidobacterium for organisms with long-term gut colonization potential. Clin. Nutr. 39:1315–1323.

Yan, X., X.-Y. Liu, D. Zhang, Y.-D. Zhang, Z.-H. Li, X. Liu, F. Wu, and G.-Q. Chen. 2021. Construction of a sustainable 3-hydroxybutyrate-producing probiotic Escherichia coli for treatment of colitis. Cell. Mol. Immunol. 18:2344–2357.

Yang, X., Y.-H. Xia, J.-Y. Wang, Y.-T. Li, Y.-F. Chang, H.-T. Chang, H.-Y. Liu, L. Chen, and C.-Q. Wang. 2020. The role of GtxA during Gallibacterium anatis infection of primary chicken oviduct epithelial cells. Mol. Cell Probes 53:101641.

Zafar, H., and M. H. Saier. 2021. Gut Bacteroides species in health and disease. Gut Microbes 13:1–20.

Zeng, P., J. Li, Y. Chen, and L. Zhang. 2019. The structures and biological functions of polysaccharides from traditional Chinese herbs. Prog. Mol. Biol. Transl. Sci. 163:423–444.

Zeng, Z., W. Yue, C. Kined, P. Wang, R. Liu, J. Liu, and X. Chen. 2023. Bacillus licheniformis reverses the environmental ceftriaxone sodium-induced gut microbial dysbiosis and intestinal inflammation in mice. Ecotoxicol. Environ. Saf. 257:114890.

Zhang, T., L. Bao, Q. Zhao, Z. E. Wu, M. Dai, Q. Rao, and F. Li. 2023. Metabolomics reveals gut microbiota contribute to PPARα deficiency-induced alcoholic liver injury. J. Proteome Res. 22:2327–2338.

Zhang, X., T. Deng, J. Lu, P. Zhao, L. Chen, M. Qian, Y. Guo, H. Qiao, Y. Xu, Y. Wang, X. Li, G. Zhang, Z. Wang, and C. Bian. 2020. Molecular characterization of variant infectious bronchitis virus in China, 2019: implications for control programmes. Transbound. Emerg. Dis. 67:1349–1355.

Zhang, Y., D. Fu, F. Yu, Q. Liu, and Z. Yu. 2011. Two catalase homologs are involved in host protection against bacterial infection and oxidative stress in Crassostrea hongkongensis. Fish Shellfish Immunol. 31:894–903.

Zhang, D.-D., H.-J. Li, H.-R. Zhang, and X.-C. Ye. 2022. Poria cocos water-soluble polysaccharide modulates anxiety-like behavior induced by sleep deprivation by regulating the gut dysbiosis, metabolic disorders and TNF-α/NF-κB signaling pathway. Food Funct. 13:6648–6664.

Zhang, G., R. D. Nichols, M. Taniguchi, T. Nakayama, and M. J. Parmely. 2003. Gamma interferon production by hepatic NK T cells during Escherichia coli infection is resistant to the inhibitory effects of oxidative stress. Infect. Immun. 71:2468–2477.

Zhang, X., Y. Zeng, Q. Qu, J. Zhu, Z. Liu, W. Ning, H. Zeng, N. Zhang, W. Du, C. Chen, and J.-A. Huang. 2017. PD-L1 induced by IFN-γ from tumor-associated macrophages via the JAK/STAT3 and PI3K/AKT signaling pathways promoted progression of lung cancer. Int. J. Clin. Oncol. 22:1026–1033.

Zhang, H., S. Zhuo, D. Song, L. Wang, J. Gu, J. Ma, Y. Gu, M. Ji, M. Chen, and Y. Guo. 2021. Icariin inhibits intestinal inflammation of DSS-induced colitis mice through modulating intestinal flora abundance and modulating p-p65/p65 molecule. Turk. J. Gastroenterol. 32:382–392.

Zhao, M., Z. Guan, N. Tang, and Y. Cheng. 2023. The differences between the water- and alkaline-soluble Poria cocos polysaccharide: a review. Int. J. Biol. Macromol. 235:123925.

Zhao, L., S. Tan, H. Zhang, P. Liu, Y.-Z. Tan, J.-C. Li, D. Jia, and X.-F. Shen. 2018. Astragalus polysaccharides exerts antiinfective activity by inducing human cathelicidin antimicrobial peptide LL-37 in respiratory epithelial cells. Phytother. Res. 32:1521–1529.

Zhao, H., L. Wu, G. Yan, Y. Chen, M. Zhou, Y. Wu, and Y. Li. 2021. Inflammation and tumor progression: signaling pathways and targeted intervention. Signal. Transduct. Target Ther. 6:263.

Zheng, H., L. Han, W. Shi, X. Fang, Y. Hong, and Y. Cao. 2022. Research advances in lotus leaf as Chinese dietary herbal medicine. Am. J. Chin. Med. 50:1423–1445.

Zhong, G., L. Li, Y. Li, F. Ma, J. Liao, Y. Li, H. Zhang, J. Pan, L. Hu, and Z. Tang. 2023. Cuproptosis is involved in copper-induced hepatotoxicity in chickens. Sci. Total Environ. 866:161458.

Zhu, H., X. Lu, L. Ling, H. Li, Y. Ou, X. Shi, Y. Lu, Y. Zhang, and D. Chen. 2018. Houttuynia cordata polysaccharides ameliorate pneumonia severity and intestinal injury in mice with influenza virus infection. J. Ethnopharmacol. 218:90–99.